Physics of Plasmas

PLEASE CITE THIS ARTICLE AS DOI: 10.1063/5.0071106

Turbulence-Driven Magnetic Reconnection and the Magnetic Correlation Length: Observations from Magnetospheric Multiscale in Earth's Magnetosheath

J. E. Stawarz,[1, a)] J. P. Eastwood,[1] T. D. Phan,[2] I. L. Gingell,[3] P. S. Pyakurel,[2] M. A. Shay,[4] S. L. Robertson,[1] C. T. Russell,[5] and O. Le Contel[6]

[1)] *Department of Physics, Imperial College London, London SW7 2AZ, UK.*

[2)] *Space Science Laboratory, University of California Berkeley, Berkeley, California 94720, USA.*

[3)] *School of Physics and Astronomy, University of Southampton, Southampton SO17 1BJ, UK.*

[4)] *Department of Physics and Astronomy, University of Delaware, Newark, Delaware 19716, USA.*

[5)] *Department of Earth, Planetary, and Space Sciences, University of California, Los Angeles, California 90095, USA*

[6)] *Laboratoire de Physique des Plasmas, CNRS, Ecole Polytechnique, Sorbonne Université, Université Paris-Saclay, Observatoire de Paris, 75252 Paris CEDEX 05, France*

(Dated: 21 November 2021)

Turbulent plasmas generate a multitude of thin current structures that can be sites for magnetic reconnection. The Magnetospheric Multiscale (MMS) mission has recently enabled the detailed examination of such turbulent current structures in Earth's magnetosheath and revealed that a novel type of reconnection, known as electron-only reconnection, can occur. In electron-only reconnection, ions do not have enough space to couple to the newly reconnected magnetic fields, suppressing ion jet formation and resulting in thinner sub-proton-scale current structures with faster super-Alfvénic electron jets. In this study, MMS observations are used to examine how the magnetic correlation length (λ_C) of the turbulence, which characterizes the size of the large-scale magnetic structures and constrains the length of the current sheets formed, influences the nature of turbulence-driven reconnection. We systematically identify 256 reconnection events across 60 intervals of magnetosheath turbulence. Most events do not appear to have ion jets; however, 18 events are identified with ion jets that are at least partially coupled to the reconnected magnetic field. The current sheet thickness and electron jet speed have a weak anti-correlation, with faster electron jets at thinner current sheets. When $\lambda_C \lesssim 20$ ion inertial lengths, as is typical near the sub-solar magnetosheath, a tendency for thinner current sheets and potentially faster electron jets is present. The results are consistent with electron-only reconnection being more prevalent for turbulent plasmas with relatively short λ_C, and may be relevant to the nonlinear dynamics and energy dissipation in turbulent plasmas.

[a)]j.stawarz@imperial.ac.uk

I. INTRODUCTION

Magnetic reconnection and turbulence are both fundamental plasma processes that have a complex and multi-faceted relationship in which reconnection jets can be a driver for turbulence[1–6] and turbulence can both generate small-scale reconnection events as an intrinsic part of the nonlinear dynamics[7–10], as well as perturb existing magnetic reconnection events[11–13]. Both phenomena are active across a wide range of plasmas throughout the Universe, including heliospheric (e.g., the solar corona[14,15], solar wind[16–19], and planetary magnetospheres[20–22]), astrophysical (e.g., the interstellar medium[23], accretion discs[24,25], and galaxy clusters[26]), and laboratory plasmas[27–29]. As such, developing an understanding of the interaction between these phenomena is a key challenge in plasma physics. In this study, we explore the behavior of turbulence-driven magnetic reconnection, occurring at the small-scale current sheets generated by the turbulent dynamics in collisionless plasmas, using the unique high-resolution measurements provided by the Magnetospheric Multiscale (MMS) mission[30] in Earth's magnetosheath.

Magnetic reconnection occurs when a change in magnetic connectivity releases stored magnetic energy and transfers it to the particles. Energy released by reconnection is partitioned across different energy channels, including the acceleration of bulk flows in the form of reconnection jets, particle heating/acceleration, and the excitation of plasma waves[31,32]. Changing the magnetic connectivity in a plasma requires breaking the frozen-in flux condition for each particle species within regions referred to as the ion diffusion region (IDR) and electron diffusion region (EDR). In collisional systems, violation of the frozen-in condition can occur through resistivity, while in the collisionless plasmas often present in space, such as Earth's magnetosheath, additional non-ideal terms in generalized Ohm's law break the frozen-in condition and cause ions and electrons to decouple from the magnetic field ($\mathbf{B}$) at different characteristic length scales[33–36]. In either case, reconnection requires small-scale gradients and, therefore, it tends to occur at thin magnetic structures, such as compressed current sheets or twisted magnetic fields. However, reconnection is fundamentally a multi-scale process, linking the small-scale dynamics associated with the thickness of the current sheet and the larger-scale dynamics associated with the length of the current sheet[7,37]. As such, depending on the process responsible for creating the current sheet, magnetic reconnection can both be responsible for driving system-scale dynamics, as in the case of the Dungey

cycle[38], solar corona[39], and large-scale solar wind current sheets[40], as well as intermediate and small-scale dynamics when formed as part of the turbulent fluctuations[9,10,41].

Turbulence is a particularly effective means of producing conditions conducive to magnetic reconnection across many systems because it naturally generates intense, small-scale gradients at a multitude of structures throughout the plasma. Within turbulent systems, nonlinear interactions exchange energy between fluctuations at different length scales. Typically energy is transferred from large to small scales on average in what is known as an energy cascade, generating an ensemble of large and small scale plasma structures in the process. The characteristic size of the largest scale fluctuations in a turbulent medium can be quantified in an average sense by the correlation length (λ_C), defined, for example for the magnetic field as

$$\lambda_C(\theta) = \int_0^\infty A(\boldsymbol{\ell})\, d\ell, \tag{1}$$

where $A(\boldsymbol{\ell})$ is the autocorrelation function defined as

$$A(\boldsymbol{\ell}) = \frac{\langle \delta\mathbf{b}(\mathbf{x}+\boldsymbol{\ell}) \cdot \delta\mathbf{b}(\mathbf{x}) \rangle}{\langle |\delta\mathbf{b}(\mathbf{x})|^2 \rangle}, \tag{2}$$

$\delta\mathbf{b} = \mathbf{B} - \langle \mathbf{B} \rangle$ is the magnetic fluctuation with zero mean, $\langle ... \rangle$ denotes a spatial average, $\boldsymbol{\ell}$ is the vector separation between two points in space, and the integral in Equation 1 is a one dimensional integral along a particular direction θ. At the smallest scales, the energy within the turbulent fluctuations is dissipated, heating and/or accelerating the particles in the plasma either through resistivity/viscosity in collisional systems or through collisionless processes[4,6,25,42–49]. Thin current sheets, as well as more complex current structures, are among the many types of structures formed in a turbulent plasma and can be potential sites for magnetic reconnection[10,50–52]. While such current sheets constitute small-scale structures in the sense that they consist of small-scale gradients in $\mathbf{B}$, the length in the other dimensions could be as large as λ_C. Turbulence-driven reconnection events can both feed energy back into the turbulent fluctuations, acting to disrupt current sheets through the plasmoid instability and acting as as one of the nonlinear couplings that exchange energy between the magnetic field and velocity fluctuations[53–59], as well as facilitate the dissipation of the turbulent fluctuations, either through processes occurring at the x-line or through secondary processes in the reconnection outflows[6,60–63].

The small-scale and disordered nature of the current sheets in a turbulent environment, in terms of location, shape, and orientation, makes the study of turbulence-driven recon-

nection challenging both with spacecraft observations and numerical simulations. Studies using two-dimensional (2D) fluid or particle-in-cell (PIC) simulations of turbulence, in which the magnetic field topology, and thus possible reconnection sites, can be straightforwardly characterized by examining the structure of a scalar magnetic potential, have demonstrated that magnetic reconnection sites spontaneously form within the turbulence and that the statistical properties of the reconnection, such as the length of the reconnecting current sheets, aspect ratio, and corresponding reconnection rates, are set by the properties of the turbulent fluctuations[8,64–66]. The identification of strong current structures in three dimensional (3D) turbulence simulations in the presence of a strong background magnetic field suggest that current sheets with X-points have different statistics than those without X-points and may contribute more to the energy dissipation than those without X-points[67]. However, in general the 3D problem is more complex with both non-sheet-like magnetic topologies[68] and arbitrary local orientations even for quasi-2D current sheets making it challenging to identify reconnection and requiring the examination of a variety of diagnostics[69].

Spacecraft observations on the other hand are limited by both the temporal resolution of the measurements and the fact that they only provide a one-dimensional trajectory, or at most a few closely spaced trajectories, through any potential reconnecting current sheet. Nonetheless, spacecraft observations have provided evidence of reconnection embedded within turbulent plasmas such as Earth's magnetosheath[63,70–73], the transition region of the Earth's bow shock[74–76], and the solar wind[41,77] by looking for plasma and electromagnetic field signatures consistent with theoretical models of quasi-2D guide field reconnection. While some of these reconnection events may be associated with larger-scale configurations of the system embedded within the turbulent plasma, it is thought that some of these events are associated with locally generated turbulent current sheets.

High-resolution measurements from MMS, which allow the detection of reconnection jets at small-scale current sheets, have provided a new opportunity to observationally examine turbulence-driven reconnection in greater detail than ever before. These observations have revealed that current sheets in Earth's turbulent magnetosheath may be undergoing a novel type of magnetic reconnection that has come to be known as electron-only reconnection[9]. Unlike the standard ion-coupled picture of reconnection, in which both electron and ion jets are accelerated by the newly reconnected magnetic field lines, in electron-only reconnection the electron jets are accelerated to super-Alfvénic speeds and the ions never couple into

the newly reconnected field lines to form ion jets either because the current sheets do not survive long enough within the dynamic turbulent environment or because the length of the current sheets along the outflow direction is not long enough for ion jets to form before the reconnected field lines fully relax. Additionally, unlike ion-coupled reconnection, in which a multi-scale structure is present normal to the current sheet with electron-scale gradients embedded within a thicker ion-scale current sheet[78], the electron-only reconnection events identified in the magnetosheath occurred at current sheets significantly thinner than the ion inertial length (d_i) and approaching several times the electron inertial length (d_e). As well as the events identified in the turbulent magnetosheath, recent MMS studies have also begun to identify reconnection events that appear to be reminiscent of electron-only reconnection in other contexts, such as at the magnetopause[79], where an apparent electron-only reconnection event was embedded within an ion scale current sheet, or in the magnetotail[80], where it has been suggested to occur during the early onset of magnetic reconnection. The varied structure of these electron-only reconnection events compared to those observed in the magnetosheath, as well as the differences in the physical constraints imposed by the system in the different plasma environments where they are found, may suggest multiple factors can lead to the occurrence of electron-only reconnection.

Idealized PIC simulations of laminar magnetic reconnection, in which the length of the reconnecting current sheets were artificially varied by changing the size of the simulation domain, have shown that if the length of the current sheet along the outflow direction is less than $\sim 40d_i$ then the ions will only partially couple to the reconnected magnetic field, resulting in reduced ion jet speeds relative to expectations, and if the the current sheet length is less than $\sim 10d_i$, the ion jets are virtually non-existent and are consistent with electron-only reconnection[78]. More recent PIC and Vlasov simulations of plasma turbulence have also begun to confirm that turbulent dynamics can generate electron-only reconnection[81–83]. The presence of electron-only reconnection in a turbulent plasma may have implications for the small-scale nonlinear dynamics of the turbulence if the reconnection begins to dominate the nonlinear timescale of the fluctuations[58,59]. In fact, analysis of the turbulent fluctuations in the intervals examined by Ref. 9, has revealed changes in the spectral power law of the magnetic field at scales comparable to the thickness of the reconnecting current sheets[10]. Additionally, if magnetic reconnection plays a significant role in energy dissipation, then the absence of ion coupling may impact how the dissipated energy is partitioned between ions

and electrons. It is, therefore, important to determine the conditions in which electron-only reconnection occurs within turbulent plasmas.

In a turbulent system, the length of the current sheets that are formed will be constrained by the size of the largest magnetic structures formed by the turbulence[8,78]. Therefore, turbulent plasmas with λ_C comparable to $10d_i$ or shorter are expected to be more conducive to electron-only reconnection than those with much larger λ_C. Values of λ_C in the two intervals examined by Ref. 9 appear to be consistent with this expectation[10]. Turbulence simulations varying the initial injection scale of the fluctuations also appear consistent, with larger injections scales producing ion-coupled reconnection and shorter injections scales producing electron-only reconnection[82]. However, examination of the properties of magnetic reconnection events across a range of turbulent intervals with varying λ_C is needed in order to observationally confirm how λ_C influences the prevalence of electron-only reconnection.

In this study, we use MMS measurements to examine how λ_C influences the nature of turbulence-driven reconnection by performing a survey of small-scale reconnection events across the dayside magnetosheath. In combination with the high-resolution, multi-point measurements provided by MMS, the relatively high densities in the magnetosheath compared to Earth's plasma sheet, as well as high temperatures relative to the solar wind, which both allow for particularly high-quality measurements of the particle distribution functions, make Earth's magnetosheath an ideal testbed for examining small-scale reconnection events[84–87]. Previous studies have demonstrated that Earth's magnetosheath contains turbulent fluctuations with early results characterising the spectrum magnetic fluctuations[88–90]. More recent studies have enabled an unprecedented examination of the detailed properties of magnetosheath turbulence – characterising the energy cascade rates of the turbulence[91,92], the electric field fluctuations[93,94] and how they are shaped by generalized Ohm's law in a turbulent plasma[36], as well as the statistics of energy conversion and dissipation at kinetic scales[48,95,96]. Statistical analyses show the properties of magnetosheath turbulence vary depending on the location and upstream conditions, providing access to variation in the plasma conditions, fluctuations properties, and, in particular for this study, λ_C[97,98].

In Sections II–IV the data, interval selection criteria, and the computation of λ_C are discussed. Section V discusses the method of systematically identifying magnetic reconection events. Section VI examines the properties of the identified reconnection events and their dependance on λ_C. Section VII discusses the potential implications of the results for

turbulent plasmas. CSV files containing the full list of turbulence intervals and reconnection events examined are provided in the Supplemental Material.

II. INTERVAL IDENTIFICATION

A survey of 60 intervals of MMS "burst" data observed between October 2015 and May 2018 are compiled. Low frequency **B** measurements are provided by the fluxgate magnetometers[99] at 128 samples/s. High frequency **B** measurements from the search-coil magnetometers[100] and electric field (**E**) measurements from the electric field double probes[101,102] are provided at 8192 samples/s. 3D particle distributions and moments for ions and electrons are measured by the Fast Plasma Investigation (FPI)[103] at 150 ms and 30 ms cadences, respectively. Where available, higher resolution particle moments[104] at 37.5 ms and 7.5 ms cadences for ions and electrons, respectively, and a merged fluxgate-searchcoil magnetic field data product[105] with cross-over frequencies between 4 and 7 Hz are used. The survey consists of intervals in which continuous burst data are available for an extended period of time, ranging from 179 to 2608 seconds. A table characterizing the average properties within each interval is provided in the supplemental material. The intervals span a range of locations in the near-equatorial magnetosheath ranging from the sub-solar point up to 132° into the flanks in the X_{GSE}–Y_{GSE} plane in geocentric solar ecliptic (GSE) coordinates. An example interval is shown in Figure 1a–g and the locations of all of the intervals in the X_{GSE}–Y_{GSE} plane is shown in Figure 3a.

The initial interval selection is based on a manual identification of continuous observations of magnetosheath burst data longer than several minutes. Intervals with obvious large-scale inhomogeneities, comparable to the size of the interval, are disregarded and the dataset is further refined by trimming or removing intervals based on an assessment of the Taylor hypothesis at the spacecraft separation scale and the convergence of the magnetic correlation length, resulting in the 60 intervals used in this study. Further details about the examination of the Taylor hypothesis and magnetic correlation lengths are discussed in Section III and Section IV, respectively, and a demonstration for the example interval is provided in Figure 1h-j.

Within each interval, the background plasma properties are characterized using temporal averages over the entire interval. Denoting the temporal average with $\langle ... \rangle$, the background

magnetic field is given by $\mathbf{B}_0 = \langle \mathbf{B} \rangle$, the background flow velocity by $\mathbf{U}_0 = \langle \mathbf{u}_i \rangle$, where $\mathbf{u}_i$ is the ion flow velocity, the background number density by $n_0 = \langle n_e \rangle$, where n_e is the electron number density and the background temperatures for species $s = i, e$ are given by $T_{s0} = \langle T_s \rangle$. Inertial lengths and gyroradii for species s are defined as $d_s = \sqrt{m_s/\mu_0 e^2 n_0}$ and $\rho_s = \sqrt{2 m_s k_B T_{s0}/e^2 B_0^2}$, respectively, where m_s is the mass of species s, μ_0 is the vacuum permeability, e is the elementary charge, and k_B is Boltzmann's constant. The plasma β for species s is defined as $\beta_s = 2\mu_0 n_0 k_B T_{s0}/B_0^2$ and the background Alfvén velocity is defined as $V_{A,0} = B_0/\sqrt{\mu_0 m_i n_0}$. Root-mean-square (rms) fluctuation amplitudes for $\mathbf{B}$ and $\mathbf{u}_i$ are given by $\delta b_{rms} = \sqrt{\langle |\mathbf{B} - \mathbf{B}_0|^2 \rangle}$ and $\delta u_{rms} = \sqrt{\langle |\mathbf{u}_i - \mathbf{U}_0|^2 \rangle}$.

The current density, $\mathbf{j}$, within the intervals can both be computed through the curl of $\mathbf{B}$ using the multi-spacecraft curlometer technique[106] and from single-spacecraft FPI moments, such that $\mathbf{j} = e n_e (\mathbf{u}_i - \mathbf{u}_e)$, where $\mathbf{u}_e$ is the electron flow velocity. When computing $\mathbf{j}$ from FPI moments, quasineutrality is assumed and $\mathbf{u}_i$ is interpolated to the resolution of the electron measurements, since currents at the smallest scales observable for the ions tend to be carried by the electrons.

III. THE TAYLOR HYPOTHESIS

The validity of the Taylor hypothesis[107], which allows the conversion of time scales into length scales, is assessed at the MMS formation size for each interval by directly comparing second-order structure functions of $\mathbf{B}$ computed using the Taylor hypothesis to those computed from the six spacecraft pairs in the formation, as shown in Figure 1h. The method builds on similar analyses employed in several previous studies[10,36,108–110]. The second-order structure function, $S_2(\boldsymbol{\ell})$, is defined as the second moment of the magnetic increments, such that

$$S_2(\boldsymbol{\ell}) = \langle |\mathbf{B}(\mathbf{x} + \boldsymbol{\ell}) - \mathbf{B}(\mathbf{x})|^2 \rangle, \tag{3}$$

where $\langle ... \rangle$ is taken to be a temporal average over an entire interval when applied to the time series spacecraft data. Observationally, Equation 3 can be evaluated at six distinct $\boldsymbol{\ell}_{Multi-S/C}$, both in terms of magnitude and orientation, by directly computing differences in $\mathbf{B}$ between the six unique spacecraft pairs in the MMS formation. For the intervals in this study, the spacecraft are typically in a regular tetrahedral formation and, therefore, $|\boldsymbol{\ell}_{Multi-S/C}|$ is generally similar, but the orientation of $\boldsymbol{\ell}_{Multi-S/C}$ significantly varies between

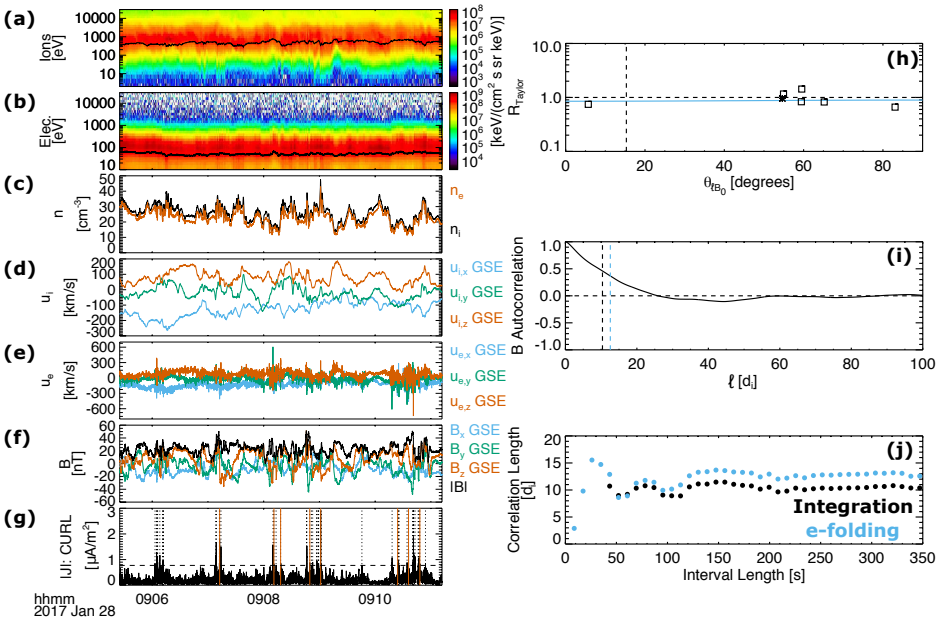

FIG. 1. Example interval of magnetosheath turbulence as observed by MMS1 showing (a) the ion differential energy flux with T_i shown as a black curve, (b) the electron differential energy flux with T_e shown as a black curve, (c) n_e and n_i, (d) $\mathbf{u}_i$, (e) $\mathbf{u}_e$, (f) the magnitude and components of $\mathbf{B}$, and (g) $|\mathbf{j}|$ computed from the curlometer. All vectors are shown in GSE coordinates. Vertical dashed lines in panel (g) mark the identified intense current structures and vertical red lines mark the identified reconnection events. (h) R_{Taylor} as a function of the angle between $\mathbf{B}_0$ and $\boldsymbol{\ell}$ (squares) for the example interval with θ_{UB} marked with a vertical dashed line. The average R_{Taylor} across all six spacecraft pairs is marked with an asterisk. A fit of the observed anisotropy to an elliptical model fixed with respect to $\mathbf{B}_0$ is shown as a solid blue curve. (i) The magnetic correlation function for the entire example interval with the estimated λ_C based on numerical integration and the e-folding distance displayed as black and blue vertical dashed lines, respectively. (j) λ_C based on numerical integration (black) and the e-folding distance (blue) for different length sub-intervals within the example interval demonstrating the convergence of the correlation length.

the different pairs. Alternatively, Equation 3 can be evaluated from a single spacecraft over a range of $|\boldsymbol{\ell}_{Taylor}|$, but at a single orientation, corresponding to the direction of $\mathbf{U}_0$,

by employing the Taylor hypothesis, such that $\boldsymbol{\ell}_{Taylor} = -\mathbf{U}_0 \Delta t$ and Δt is the temporal separation between two data points.

For each $|\boldsymbol{\ell}_{Multi-S/C}|$ in the formation, the equivalent $|\boldsymbol{\ell}_{Taylor}|$ is determined and the ratio $R_{Taylor} = S_2\left(\boldsymbol{\ell}_{Multi-S/C}\right)/S_2\left(\boldsymbol{\ell}_{Taylor}\right)$ is computed. If the Taylor hypothesis is valid at the scales $|\boldsymbol{\ell}_{Multi-S/C}|$, R_{Taylor} will normalize out the overall variation of S_2 as a function of $|\boldsymbol{\ell}|$, but may vary as a function of the angle $\cos\left(\theta_\ell\right) = \boldsymbol{\ell}_{Multi-S/C} \cdot \mathbf{U}_0 / |\boldsymbol{\ell}_{Multi-S/C}||\mathbf{U}_0|$ due to the anisotropy of $S_2\left(\boldsymbol{\ell}\right)$ and will be unity along the direction of $\mathbf{U}_0$. For isotropic turbulence, R_{Taylor} will be constant as a function of θ_ℓ. However, for a plasma in the presence of a significant global $\mathbf{B}_0$ over the interval the turbulence would typically be expected to be anisotropic with larger values for $S_2\left(\boldsymbol{\ell}\right)$ perpendicular to $\mathbf{B}_0$ and smaller values along $\mathbf{B}_0$. Assuming the fluctuations are statistically isotropic in the plane perpendicular to the global $\mathbf{B}_0$, R_{Taylor} would then be expected to increase as a function of $\theta_{\ell B_0} = \boldsymbol{\ell}_{Multi-S/C} \cdot \mathbf{B}_0 / |\boldsymbol{\ell}_{Multi-S/C}||\mathbf{B}_0|$ and equal one when $\theta_{\ell B_0} = \theta_{UB}$, where θ_{UB} is the angle between $\mathbf{U}_0$ and $\mathbf{B}_0$.

In this study, R_{Taylor} is typically found to be consistent with isotropy, as seen in Figure 1h, or to have an increasing trend with angles more field-aligned than $\mathbf{U}_0$ less than unity and angles less field-aligned than $\mathbf{U}_0$ greater than unity, as seen for three example intervals with different orientations of $\mathbf{U}_0$ relative to $\mathbf{B}_0$ in Figure 2a-c, consistent with the anisotropy expected in the presence of a large $\mathbf{B}_0$. The presence of a subset of intervals that are consistent with isotropy relative to the global $\mathbf{B}_0$ is expected, since $\delta b_{rms}/B_0$ is often larger than unity in the magnetosheath (see supplemental material). For each of the intervals analysed in this study, we fit the observed values of R_{Taylor} to a simple ellipsoidal model of the anisotropy in $\sqrt{S_2\left(\boldsymbol{\ell}\right)}$, such that

$$R_{Taylor}\left(\theta_\ell\right) = \frac{1}{c_1 + c_2 \cos^2\left(\theta_{\ell B_0}\right)}, \tag{4}$$

where c_1 and c_2 are fitting parameters quantifying the degree of anisotropy. The functional form in Equation 4 is simply selected as a relatively simple model that empirically appeared to fit the variation in the data reasonably well. Figure 2d shows the degree of anisotropy as quantified by $(c_1+c_2)/c_1$ as a function of $\delta b_{rms}/B_0$ for each interval, demonstrating isotropic intervals tend to occur when $\delta b_{rms}/B_0 > 1$ and more anisotropic intervals with R_{Taylor} or S_2 elongated perpendicular to $\mathbf{B}_0$ tend to occur when $\delta b_{rms}/B_0$ is small. This organisation of the variability in R_{Taylor} as a function of $\theta_{\ell B_0}$ in a manner consistent with the expectations

from turbulence theory suggest that much of the variation in the estimates of $S_2\left(\boldsymbol{\ell}_{Multi-S/C}\right)$ is a physical signal. In this analysis, we focus on examining the anisotropy with respect to the global $\mathbf{B}_0$ over the entire interval since we are using it to aid with validating the Taylor hypothesis for use in estimating λ_C, which is a large-scale property of the fluctuations; however, in principle, one would also expect that in the large $\delta b_{rms}/B_0 > 1$ intervals, the anisotropy of the turbulence would be organised with respect to a locally defined magnetic field[80,111].

To check the validity of the Taylor hypothesis, the average value of the observed R_{Taylor} within $\pm 5^\circ$ of $\mathbf{U}_0$ is computed and the Taylor hypothesis is considered reasonably well satisfied if this average along the flow direction is within a factor of two of unity. If no spacecraft in the formation are separated along a direction within $\pm 5^\circ$ of $\mathbf{U}_0$, then the Taylor hypothesis is considered reasonably satisfied if the value of the fit to Equation 4 along the direction of $\mathbf{U}_0$ is within a factor of two of unity. The intervals analyzed in this study are typically well within the factor of two threshold, with an average of 1.11 ± 0.25. Since the Taylor hypothesis is satisfied at the scale of the spacecraft separation, it is a reasonable assumption that it is also valid at larger scales, where phase velocities are typically slower. As such, the Taylor hypothesis can be used to estimate λ_C which requires information about the fluctuations across multiple scales that are not directly accessible from the tetrahedral formation.

IV. MAGNETIC CORRELATION LENGTHS

The characteristic length scale of the largest magnetic structures within a turbulent environment can be quantified by λ_C, based on the autocorrelation function of $\mathbf{B}$ as defined in Equation 2. As with $S_2(\boldsymbol{\ell})$, when computing $A(\boldsymbol{\ell})$ from time series spacecraft data the average is taken to be a temporal average over an entire interval. Within a turbulent environment, $A(\boldsymbol{\ell})$ is expected to decrease from a value of one by definition at $\boldsymbol{\ell} = 0$ to zero as $\boldsymbol{\ell} \to \pm\infty$. This approximate behavior is observed in all of the intervals examined in this study, as can be seen for the example interval in Figure 1i. The length scale over which the decrease in $A(\boldsymbol{\ell})$ occurs is characterized by λ_C and can be computed by integrating over the autocorrelation function in accordance with Equation 1. When estimating λ_C from the observational data, a numerical integration is performed between $\ell_{Taylor} = 0$ and the ℓ_{Taylor}

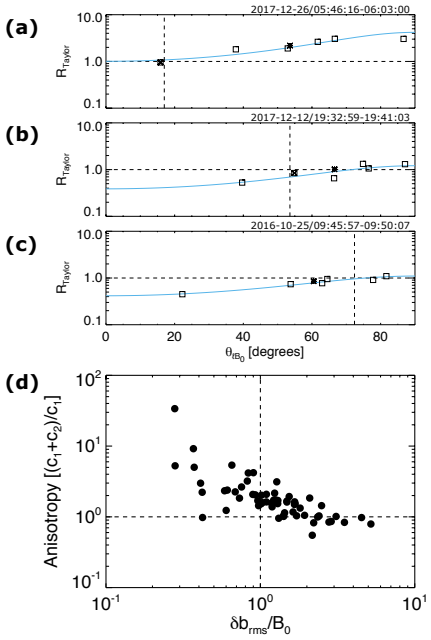

FIG. 2. (a-c) R_{Taylor} as a function of the angle between $\mathbf{B}_0$ and $\boldsymbol{\ell}$ in the same format as Figure 1h for three example intervals with different θ_{UB} that have evidence of anisotropy with respect to the background magnetic field. Each interval has $R_{Taylor} \sim 1$ along θ_{UB} (dashed vertical line) with an increasing trend from 0° to 90° that is fit to an elliptical model fixed with respect to $\mathbf{B}_0$ (solid blue curve). (d) The degree of anisotropy in the model fit as a function of $\delta b_{rms}/B_0$ for all 60 intervals examined in this study, showing decreasing anisotropy with respect to the global $\mathbf{B}_0$ for the intervals as $\delta b_{rms}/B_0$ increased. Values of one indicate isotropy, values greater than one indicate S_2 is elongated perpendicular to $\mathbf{B}_0$, and values less than one indicate S_2 is elongated parallel to $\mathbf{B}_0$.

at which the first zero crossing of $A\left(\boldsymbol{\ell}_{Taylor}\right)$ occurs since $A\left(\boldsymbol{\ell}_{Taylor}\right)$ tends to oscillate about zero at a low amplitude for large ℓ_{Taylor}. Another commonly used estimate of λ_C is to find the distance over which $A\left(\boldsymbol{\ell}_{Taylor}\right)$ decreases by one e-folding (i.e., a factor of $1/e \sim 0.37$), which is equivalent to Equation 1 if $A\left(\boldsymbol{\ell}_{Taylor}\right)$ is an exponential[20,112]. For the intervals examined in this study, both methods typically give similar estimates of λ_C, as seen in Figure 1i.

In general $A\left(\boldsymbol{\ell}\right)$ can be an anisotropic function and in the presence of a background

magnetic field, λ_C is expected to be longer along $\mathbf{B}_0$ and shorter perpendicular to $\mathbf{B}_0$. When measuring $A(\boldsymbol{\ell}_{Taylor})$, as done in this study, $\boldsymbol{\ell}_{Taylor}$ is only sampled along the direction of $\mathbf{U}_0$ and, thus, λ_C may vary between different intervals due to an overall change in the size of magnetic structures within the region and/or due to a difference in the angle, θ_{UB}, between $\mathbf{U}_0$ and $\mathbf{B}_0$.

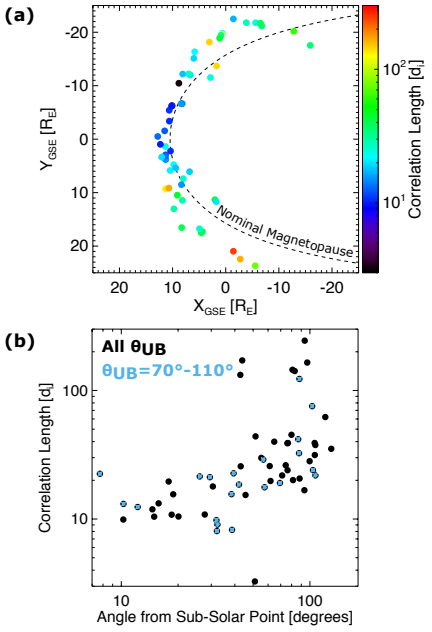

FIG. 3. (a) Location in the $X_{GSE}-Y_{GSE}$ plane of each magnetosheath turbulence interval examined in this study with colors representing λ_C as estimated from numerical integration using the entire turbulence interval. A nominal magnetopause location based on the Shue model[113] is shown as a dashed curve. (b) λ_C estimated from numerical integration as a function of the angle away from the sub-solar point with intervals for which the angle between $\mathbf{B}_0$ and $\mathbf{U}_0$ is within $\pm 20°$ of perpendicular shown as blue asterisks.

Values of λ_C are estimated for all 60 intervals of magnetosheath turbulence examined in this study. For each interval, the convergence of the estimated λ_C is examined by computing λ_C for subintervals which began at the start time of the interval and extended to a specified fraction of the total interval. A series of such subintervals are examined with increasing

duration and λ_C is plotted as a function of the subinterval length, as seen for the example interval in Figure 1j. The intervals analyzed in this study are partly selected such that the correlation lengths appeared to reasonably converge upon visual inspection, which provides some confidence that the intervals are homogeneous/stationary in a statistical sense. For the following analysis, λ_C is taken as the value computed from the entire interval.

As seen in Figure 3, which shows λ_C for each interval as a function of the location, a clear trend is present with shorter λ_C near the sub-solar magnetosheath and longer λ_C toward the flanks. Similar general behavior has also been reported from Cluster data[97]. Values of λ_C vary from $\sim 10d_i$ near the sub-solar point to $\sim 200d_i$, but more typically $\sim 40d_i$, in the flanks at $\sim 120°$ from the sub-solar point. These values span the range of current sheet lengths over which reconnection is expected to transition from ion-coupled to electron-only reconnection based on idealized simulations[78]. The value of θ_{UB} has a relatively uniform distribution between 0° and 180° for the 60 intervals in this study and no clear relationship is apparent between θ_{UB} and λ_C. Restricting the examination of λ_C to only those intervals for which θ_{UB} is within 20° of perpendicular (light blue points in Figure 3b), thus indicating that the perpendicular correlation length is estimated from the Taylor hypothesis, shows a similar relationship between λ_C and location, with shorter λ_C near the sub-solar magnetosheath and longer λ_C on the flanks. The trend in λ_C is, therefore, not purely an artefact of differences in the average θ_{UB} between the sub-solar point and flanks and there are, in fact, larger scale magnetic structures in the flanks. We next investigate whether there is a difference in the properties of magnetic reconnection events between the sub-solar magnetosheath and flanks.

V. RECONNECTION EVENT IDENTIFICATION

All 60 intervals are systematically examined for evidence of small-scale reconnection using a partially automated process, which involves:

1. Identifying distinct current structures within the intervals
2. Rotating each current structure into a local current-sheet-oriented (LMN) coordinate system
3. Checking for a reversal in the B_L component of the magnetic field
4. Checking for a perturbation in the $u_{e,L}$ component of the electron flow

5. Manually verifying the reconnection events

Distinct current structures within the intervals are identified using a method similar to Ref. 10, in which local maxima in $|\mathbf{j}|$ above a given threshold are located. Adjacent local maxima are considered independent current structures if the local minimum between them is less than the half-maximum of both local maxima, otherwise both peaks are merged into a single structure. The half-maximum locations and location of the peak $|\mathbf{j}|$ are then recorded for each current structure. The location of the identified current structures in the example interval are marked with vertical dotted lines in Figure 1g. Current structures are initially identified using the higher time resolution curlometer derived $\mathbf{j}$, which, while it is effectively smoothed over the formation size, does well at capturing the range of time over which a given structure is observed by all four spacecraft. For each current structure, the peak and half-maximum locations of each individual spacecraft encounter are identified using the lower resolution FPI derived $\mathbf{j}$ based on the location and extent of the curlometer identified structure. A linear interpolation between data points is used to compute the half-maximum locations for the FPI derived $\mathbf{j}$. The threshold used to identify current structures is taken as 3 times the rms $|\mathbf{j}|$ for each interval. The current structure identification results in 2505 intense current structures across all of the intervals.

Once identified, the current structures are rotated into a local LMN coordinate system based on a hybrid minimum variance analysis (HMVA) method[114], such that

$$\hat{\mathbf{N}} = \hat{\mathbf{b}}_1 \times \hat{\mathbf{b}}_2, \qquad \hat{\mathbf{M}} = \hat{\mathbf{x}}_{max} \times \hat{\mathbf{N}}, \qquad \hat{\mathbf{L}} = \hat{\mathbf{M}} \times \hat{\mathbf{N}}, \tag{5}$$

where $\hat{\mathbf{b}}_1$ and $\hat{\mathbf{b}}_2$ are the magnetic field directions on either side of the current structure and $\hat{\mathbf{x}}_{max}$ is the maximum variance direction of $\mathbf{B}$ obtained from minimum variance analysis (MVA) . In this coordinate system, for a current-sheet-like structure, $\hat{\mathbf{N}}$ is the normal to the current sheet, $\hat{\mathbf{M}}$ is the guide field direction, and, if the current sheet is reconnecting, $\hat{\mathbf{L}}$ is the outflow direction. Unit vectors $\hat{\mathbf{b}}_1$ and $\hat{\mathbf{b}}_2$ are taken to be the magnetic field directions at the start and end times of the interval over which MVA is performed. Multiple potential MVA time intervals are examined for each event with interval lengths of 1×, 1.5×, and 2× the temporal half-maximum width on either side of the current signature. This procedure is performed for the events as observed by each spacecraft, resulting in 12 potential LMN coordinate systems for each structure (3 coordinate systems based on the temporal half-maximum widths and magnetic field profiles observed by each of the 4 spacecraft). Of the

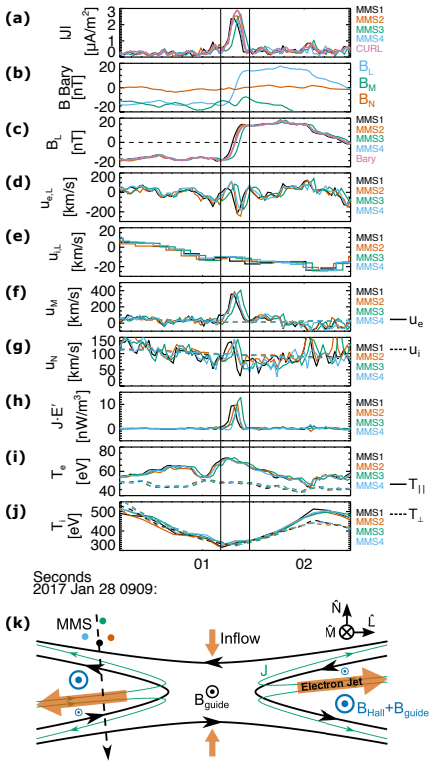

FIG. 4. An example of a reconnection event without a clear ion jet in a local LMN coordinate system for the current sheet. (a) $|\mathbf{j}|$ as computed from FPI for each spacecraft and from the curlometer, (b) $\mathbf{B}$ averaged to the barycenter of the MMS formation, (c) B_L as observed by each spacecraft and averaged to the barycenter of the formation, (d) $\mathbf{u}_{eL}$ as observed by each spacecraft, (e) $\mathbf{u}_{iL}$ as observed by each spacecraft, (f) $\mathbf{u}_M$ for electrons (solid) and ions (dashed) as observed by each spacecraft, (g) $\mathbf{u}_N$ for electrons (solid) and ions (dashed) as observed by each spacecraft, (h) energy conversion between the electromagnetic fields and particles as quantified by $\mathbf{j}\cdot\mathbf{E}' = \mathbf{j}\cdot(\mathbf{E}+\mathbf{u}_e\times\mathbf{B})$ as computed using the FPI $\mathbf{j}$ for each spacecraft, (i) the parallel (solid) and perpendicular (dashed) electron temperature, and (j) the parallel (solid) and perpendicular (dashed) ion temperature. Vertical solid lines mark the extent of the current sheet across the four spacecraft. (k) Diagram of the inferred trajectory of MMS through the reconnection event.

12 potential coordinate systems, the LMN coordinate system giving the most symmetric B_L profile about zero, if a B_L reversal is present, is selected and, for any given structure, a single coordinate system is used for all spacecraft.

For the traversal of a sheet-like reconnection outflow, a reversal in B_L (e.g., Figure 4c) is expected and a flow perturbation in the $\hat{\mathbf{L}}$ direction will be present within the current sheet (e.g., Figure 4d). For ion-coupled reconnection, the flow perturbation will be present in both $u_{e,L}$ and $u_{i,L}$, while for electron-only reconnection or events where the spacecraft encountered the ion diffusion region, a $u_{e,L}$ perturbation will be present and the $u_{i,L}$ perturbation may be weak or non-existent. Therefore, the presence of a B_L reversal and $u_{e,L}$ perturbation within the current structures are used as checks for possible magnetic reconnection events. A threshold on the $u_{e,L}$ perturbation, motivated by Ref. 115, is set at $0.7\Delta V_{A,L}$, where $\Delta V_{A,L}$ is the average change in the $\hat{\mathbf{L}}$ component of the Alfvén velocity, $V_{A,L} = B_L/\sqrt{\mu_0 n_e m_i}$, between either edge of the current sheet and the location where B_L changes sign. This threshold should capture both ion-Alfvénic electron jets, which may be present in ion-coupled reconnection, and super-ion-Alfvénic electron jets which are expected in electron-only reconnection. In the presence of a guide field, the Lorentz force can deflect the electron outflows toward one side of the current sheet[116], which complicates the typical Walén test, in which a reversal in the correlation between the velocity perturbation and the magnetic field is looked for. Therefore, a Walén test is not incorporated into the automated portion of the reconnection event identification. These criteria result in an over-selection of potential reconnection events and a manual inspection and refinement of each event is performed to select those which appear most consistent with reconnection. This procedure results in the identification of 256 events or $\sim 10\%$ of the observed intense current structures undergoing reconnection. Based on the length of each turbulent interval, roughly one reconnection event is observed every two minutes on average in the dataset. The locations of the observed reconnection events in the example interval are marked with solid red lines in Figure 1g.

The possible presence of ion jets in the reconnection events is assessed by examining the Walén relationship between $\Delta V_{A,L}$ and $\Delta u_{i,L}$, in which a change in correlation between these two quantities is expected within the current sheet for a reconnection-driven ion jet. In examining the Walén relationship, $V_{A,L}$ is averaged to the either 150 ms or 37.5 ms resolution of the ion measurements and the profile in time of $\Delta V_{A,L}$ and $\Delta u_{i,L}$ are computed

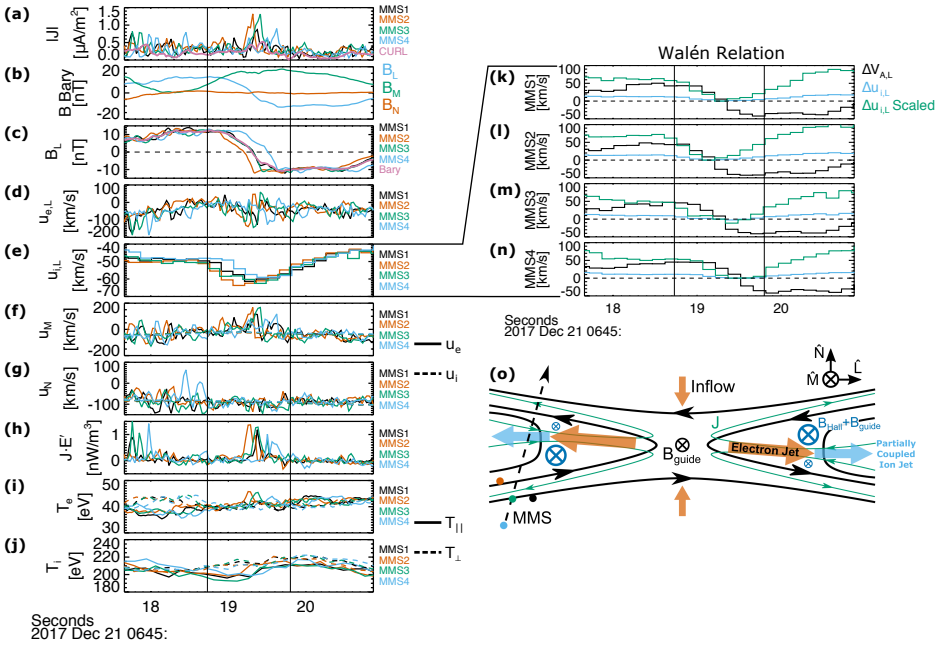

FIG. 5. Example reconnection event with a clear ion jet with (a-j) in the same format as Figure 4a–j. (h-k) examine the Walén relation for the ion jet as observed by each spacecraft by comparing $\Delta V_{A,L} = V_{A,L} - V_{AL,ref}$ averaged to the resolution of the ion measurements (black) to $\Delta u_{i,L} = u_{i,L} - u_{iL,ref}$ (blue), where $V_{AL,ref}$ and $u_{iL,ref}$ are taken to be the values at the time where B_L crosses zero. Green curves are the same as the blue curves in (k-n) but scaled by a factor of ~ 5, such that the profile of $\Delta u_{i,L}$ for the partially coupled ion jet is more clear in comparison with $\Delta V_{A,L}$. As is apparent for all four spacecraft in this example event, for a fully or partially coupled ion jet, a reversal in correlation between $\Delta u_{i,L}$ and $\Delta V_{A,L}$ is expected that is centered at the time of the zero crossing in $\Delta V_{A,L}$. (o) Diagram of the inferred trajectory of MMS through the reconnection event.

relative to the reference time at which B_L crosses zero within the current sheet for each spacecraft. Analyzed in this way, the peak velocity of an ion jet is expected to occur at the location where $\Delta V_{A,L}$ reverses sign, resulting in $\Delta u_{i,L} \sim 0$ since $\Delta u_{i,L}$ is computed relative to that location, and the correlation between $\Delta u_{i,L}$ and $\Delta V_{A,L}$ within the current sheet will reverse sign on either side of this point. For a fully coupled ion jet, assuming

a significant temperature anisotropy is not present, the amplitude of $\Delta u_{i,L}$ is expected to be comparable to the amplitude of $\Delta V_{A,L}$ within the current sheet. However, for ion flows that are only partially coupled to $\mathbf{B}$, as can occur in the ion diffusion region or for current sheets with lengths in the range where ion-coupled reconnection transitions to electron-only reconnection, $\Delta u_{i,L}$ can be significantly lower amplitude than $\Delta V_{A,L}$[78], as seen for the example event in Figure 5k–n. As such, the key feature used to identify either fully or partially coupled ion jets is a clear reversal in correlation between $\Delta u_{i,L}$ and $\Delta V_{A,L}$ at approximately the location of the $\Delta V_{A,L}$ reversal. Overall, 18 clear ion jets are identified out of the 256 reconnection events using this analysis.

The use of these criteria for identifying reconnection events, which are based on the standard 2D picture of guide field reconnection, likely limits the reconnection events identified to those which occur at almost sheet-like current structures, at least on the scale over which the spacecraft traverse the current sheets, which is $\sim$ 45 km in the L direction and $\sim$ 59 km in the M direction on average, assuming the reconnection events are advected in the local background plasma plasma flow as estimated from the average ion velocity over 10 d_i surrounding each event. It is possible that complex magnetic topologies within a turbulent environment can also give rise to more complicated 3D current structures that may or may not also undergo reconnection[68,69]. There may also be additional reconnection events at current sheets with lower amplitudes than 3 times the rms $|\mathbf{j}|$ that are not captured by the analysis. However, even so, a significant number of reconnection events spanning a range of scales are identified using the present criteria and provide a good starting point for the systematic observational examination of turbulence-driven reconnection.

In the following analysis, the velocity of the structures over the spacecraft is estimated as the ion flow averaged over 10 d_i surrounding each event ($\langle \mathbf{u}_i \rangle_{10d_i}$), which is equivalent to assuming the reconnection events are advected over the spacecraft by the local background plasma flow, as opposed to propagating with respect to the plasma. Different averaging scales ranging from $10d_i$ to $100d_i$ surrounding each event, as well as, the average velocity over the entire turbulent interval (i.e., $\mathbf{U}_0$) have also been examined and, while they vary with respect to $\langle \mathbf{u}_i \rangle_{10d_i}$, they produce roughly consistent velocities and do not qualitatively alter the results presented in the following sections. Normal components of the current sheet motion based on multi-spacecraft timing analysis[117] on the zero crossing of B_L for the subset of events where the analysis could be reasonably performed have also been examined. The

results from the timing analysis are roughly consistent with those obtained from $\langle \mathbf{u}_i \rangle_{10d_i}$ for most events. Normal speeds obtained from the timing analysis are typically within 16% of $|\langle u_{i,N} \rangle_{10d_i}|$ as quantified by the median difference between the values across the events and are roughly centred on the values estimated from $|\langle u_{i,N} \rangle_{10d_i}|$, consistent with the assumption that the structures are advected in the background plasma flow. The normal directions of the current sheets are also in good agreement with those obtained from HMVA, with angular differences between the two within 20° for the vast majority of events. Since the $\langle \mathbf{u}_i \rangle_{10d_i}$ procedure can be easily applied to all of the identified reconnection events and because timing analysis also has its own set of limitations (i.e., assuming a planar structure, constant velocity, etc.), we opt to present the results based on $\langle \mathbf{u}_i \rangle_{10d_i}$. However, the results obtained from multi-spacecraft timing are qualitatively consistent with those presented in the following sections.

VI. RECONNECTION EVENT PROPERTIES

A. Electron-Only and Ion-Coupled Reconnection Events

Figure 4 shows an example of an event for which an ion jet was not observed and a diagram of the inferred spatial structure with the trajectory of MMS through the event. A strong current is present (Figure 4a), which is carried by a strong out-of-plane $u_{e,M}$ electron flow (Figure 4f). A negative to positive B_L reversal (Figure 4c) is observed by all four spacecraft in conjunction with a negative $u_{e,L}$ electron jet (Figure 4d), indicating the x-line is located in the $+\hat{\mathbf{L}}$ direction relative to MMS as illustrated in Figure 4k. A negative B_M guide field (Figure 4b) is present throughout the event along with a bipolar negative to positive B_M perturbation relative to the guide field within the current sheet, as expected from the Hall effect in a reconnecting current sheet. The polarity of the Hall perturbation is consistent with the reconnection event being advected by the background flow in $+\hat{\mathbf{N}}$ over the spacecraft, consistent with the positive $u_{i,N}$ throughout the event (Figure 4g). In the presence of a guide field, a Lorentz force given by $-\mathbf{u}_e \times \mathbf{B}_{guide}/(en_e)$ acts to deflect the electron jet in the $\hat{\mathbf{N}}$ direction[116]. For this event, the electron jet is expected to be deflected toward the side of the current sheet with positive B_L, consistent with the timing of the peak in the electron jet relative to the sign change in B_L. A clear signature of energy

exchange from the electromagnetic fields into the particles is present, as indicated by a positive $\mathbf{j} \cdot \mathbf{E}' = \mathbf{j} \cdot (\mathbf{E} + \mathbf{u}_e \times \mathbf{B})$ within the current sheet (Figure 4h). The event is located within a larger-scale increase in the parallel electron temperature (Figure 4i) and a decrease in both the parallel and perpendicular ion temperature (Figure 4j); however, since these temperature signatures occur over a larger scale than the reconnection event, it is not clear that they are directly associated with the reconnection. Multi-spacecraft timing analysis on the zero crossing of the B_L profile for the event gives a speed in the direction normal to the current sheet of $\sim$ 81 km, which is roughly consistent with the average ion flow over $10d_i$ surrounding the event of $\sim$ 100 km/s. Additionally, the normal direction of the current sheet obtained from the timing analysis has an angular difference within 14° of that obtained from HMVA.

An example of an ion-coupled reconnection event along with a diagram of the inferred structure and MMS trajectory is provided in Figure 5. Again, a strong current is observed by all four spacecraft (Figure 5a) carried by a $u_{e,M}$ electron flow. However, in this case two enhancements of the current are observed within the overall B_L reversal, with an initial weak enhancement followed by the stronger current, potentially indicating a bifurcated current sheet. A reduction of the slope inside of the B_L reversal, flanked on either side by steeper slopes, is also consistent with a weak bifurcation[118]. Negative $u_{e,L}$ (Figure 5d) and $u_{i,L}$ (Figure 5e) jet signatures are present again indicating the x-line is in the $+\hat{\mathbf{L}}$ direction relative to spacecraft as shown in Figure 5o. A clear difference in the time of the B_L reversal is present between the spacecraft, first being observed by MMS2 followed by MMS1 and MMS3 at nearly the same time and then finally MMS4, which is consistent with the differences in the times between the peak ion and electron jet velocities. Multi-spacecraft timing analysis on the zero crossing of the B_L profile again provides normal components of the motion roughly consistent with those estimated from $\langle u_{i,N} \rangle_{10d_i}$ ($\sim$ 110 km/s compared to $\langle u_{i,N} \rangle_{10d_i} \sim$ 90 km/s) and a normal direction for the current sheet within 14° of that obtained from HMVA. In this case, while the electron jet is super-Alfvénic with $\Delta u_{e,L} \sim 3.7 \Delta V_{A,L}$, the ion jet is somewhat sub-Alfvénic with $\Delta u_{i,L} \sim 0.2 \Delta V_{A,L}$, which may be consistent with the current sheet having an overall length short enough to be in the transition range between ion-coupled and electron-only reconnection, such that the ions only have enough space to partially couple to the field, or with crossing the event within the IDR at a location where the ions have only partially coupled to the reconnected magnetic field. On the trailing side

of this event, the jet profile in $u_{i,L}$ potentially extends beyond the current sheet and similar behaviour on one or both sides of the current sheets is also observed in 6 of the 18 other events with ion jets. Whether this seeming extension of the ion jet beyond the current sheet is simply associated with the turbulent background velocities that these events are embedded within or are actually a feature of the ion jets remains unclear; however, similar behavior has been reported in the IDR for reconnection events in other contexts[119]. A positive B_M guide field with a positive followed by negative Hall perturbation (Figure 5b) is present within the current sheet, consistent with the event being advected in the $-\hat{\mathbf{N}}$ direction over the spacecraft, as expected from the negative $u_{i,N}$ velocities in the event (Figure 5g). Clear positive enhancements in $\mathbf{j} \cdot \mathbf{E}'$ (Figure 5h) are again observed, indicating energy exchange from the electromagnetic fields to the particles. Background electron (Figure 5i) and ion (Figure 5j) temperatures are nearly constant and isotropic across the event; however, clear enhancements in the parallel electron temperatures of $\sim$ 5eV are present in conjunction with the $\mathbf{j} \cdot \mathbf{E}'$ signatures. The duration of these $\mathbf{j} \cdot \mathbf{E}'$ and temperature signatures are thinner than the accompanying ion jet, suggesting sub-structure is present in the outflows. While such enhancements in the temperature are present in some of the events, the majority of events do not have obvious signatures that might be associated with heating.

B. Current Sheet and Reconnection Jet Properties

Many of the reconnection events have significant guide fields, which can impact the amount of magnetic energy available to reconnect and nature of the particle energization associated with the magnetic reconnection[63]. For each reconnection event, the shear angle of the magnetic field across the current sheet is defined as

$$\theta_{shear} = \arccos\left(\frac{\mathbf{B}_1 \cdot \mathbf{B}_2}{|\mathbf{B}_1||\mathbf{B}_2|}\right), \tag{6}$$

where $\mathbf{B}_1$ and $\mathbf{B}_2$ are the magnetic field on either side of the current sheet and the ratio of the guide field to the reconnecting component of the field can be estimated as $B_{guide}/B_{rec} = [\tan(\theta_{shear}/2)]^{-1}$ (c.f., Refs. 120 and 121). The distribution of B_{guide}/B_{rec} for each reconnection event is displayed in Figure 6a. A similar distribution is also obtained if B_{guide}/B_{rec} is estimated as the ratio of $|B_M|$ at the location of the B_L reversal to the average $|B_L|$ on either side of the current sheet. While there is a population of reconnection

events with larger B_{rec} than B_{guide}, the majority of events have B_{guide}/B_{rec} between 1 and 10, consistent with magnetic shears between 10° and 90°.

For asymmetric guide field reconnection, the inflow Alfvén speed is given by[122,123]

$$V_{A,inflow} = \sqrt{\frac{|B_{L,1}||B_{L,2}|\left(|B_{L,1}| + |B_{L,2}|\right)}{\mu_0 m_i \left(n_1|B_{L,2}| + n_2|B_{L,1}|\right)}} \tag{7}$$

where $B_{L,1}$ and $B_{L,2}$ are the L-components of the magnetic field on either side of the current sheet and n_1 and n_2 are the number densities on either side of the current sheet. The available magnetic energy per electron-proton pair that can be released by reconnection is $m_i V_{A,inflow}^2$[124,125]. Through reconnection, this energy is redistributed into the acceleration of ion and electron jets, the heating of particles, and the excitation of waves and other small-scale plasma structures. The distribution of $m_i V_{A,inflow}^2$ observed for each reconnection event averaged across the four spacecraft is shown in Figure 6b and varies from $\sim$ 1eV to 100eV per electron-proton pair. Given that only a fraction of this energy is converted into plasma heating[124,125], this likely explains why only a fraction of events have clear signature of particle heating, with larger $m_i V_{A,inflow}^2$ events having the opportunity to provide more obvious signatures of heating relative to the several tens of eV background temperatures of electrons and several hundred eV background temperatures of the ions.

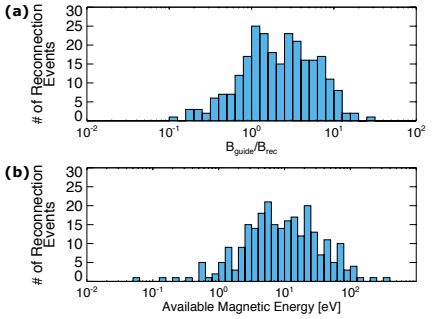

FIG. 6. Histograms of (a) the ratio between the strength of the guide field (B_M) and reconnecting component of the field (B_L) for each event, related to the magnetic shear angle across the current sheet by $B_{rec}/B_{guide} = \tan(\theta_{shear}/2)$, and (b) the available magnetic energy per electron-proton pair given by $m_i V_{A,inflow}^2$ for each reconnection event.

Figure 7a shows the observed current sheet thicknesses and peak electron and ion jet velocities for each of the reconnection events. The full temporal width, Δt_{CS}, of each

event is manually identified for each spacecraft and the spatial thickness is estimated as $|\langle u_{i,N}\rangle_{10d_i}|\Delta t_{CS}$. In Figure 7a and the subsequent analysis, the current sheet thickness is estimated from the spacecraft that observed the strongest current. Ion and electron jet velocities are quantified as the largest $|\Delta u_{i,L}|$ and $|\Delta u_{e,L}|$, respectively, within the current sheet relative to the average velocity observed on either side of the current sheet, expressed in units of $|\Delta V_{A,L}|$ between the peak jet velocity and the edges of the event. The largest $|\Delta u_L|/|\Delta V_{A,L}|$ across the four spacecraft is used to quantify the jet velocities for each event.

Current sheet thicknesses span from $\sim d_e$ to a few d_i, with 56% of the events having thicknesses $< d_i$. The majority of events have no clear evidence of ion jets and those that do tend to occur at ion scale current sheets with thicknesses $> d_i$, consistent with the typical picture of ion-coupled magnetic reconnection. The observed ion jets tend to be Alfvénic or sub-Alfvénic with observed peak velocities below $\Delta V_{A,L}$, while electron jet velocities tend to be super-Alfvénic with velocities extending to nearly $40\Delta V_{A,L}$, comparable to the Alfvén speed based on the electron mass. A weak correlation is present between the observed thicknesses and peak electron jet velocities, with ion-scale current sheets having electron jet speeds closer to $\Delta V_{A,L}$ and faster electron jets observed for the thinner sub-proton-scale current sheets.

The lack of clear ion jets in any given event could result from MMS encountering IDR, such that ion jets are not observed but could be present further along the outflow direction. Alternatively, the lack of ion jets could result from electron-only reconnection, in which there is not enough space for the ion jets to form at all before the reconnected field lines relax. As noted by Ref. 9, the volume of space occupied by the ion jets in ion-coupled reconnection is expected to be much larger than the volume of space occupied by the IDR and, therefore, one would expect to more commonly encounter the ion jets than the IDR if events are randomly sampled in a turbulent environment. The relative lack of ion jets, only 18 observed out of 256 events, compared to electron jets may suggest that electron-only reconnection is occurring. This interpretation could also be influenced by the lower temporal resolution of the ion measurements. However, 89% of events have Δt_{CS} greater than even the larger 150 ms ion resolution and 82% of events with sub-proton-scale current sheet thicknesses have $\Delta t_{CS} > 150$ ms, suggesting ion jets could have been detected for most of the current sheets if they were present.

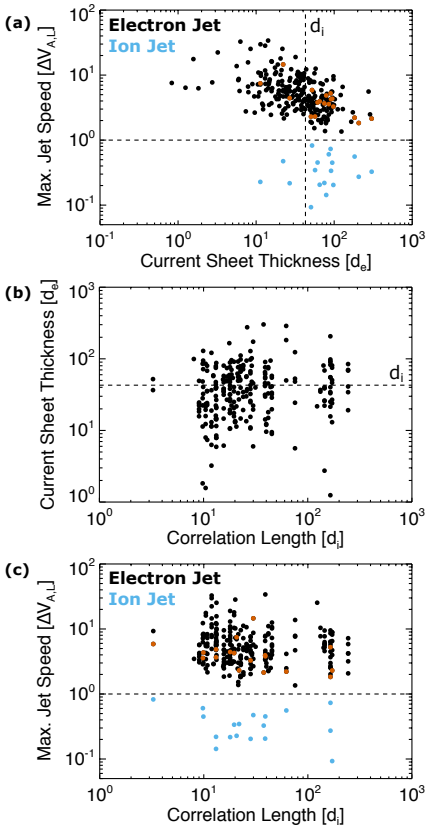

FIG. 7. (a) Comparison of the thickness of the reconnecting current sheets and the peak $\Delta u_{e,L}$ (black) and $\Delta u_{i,L}$ (blue) jet velocities in units of $\Delta V_{A,L}$ between the center and edges of the current sheet. (b) Relationship between the thickness of the reconnecting current sheets and λ_C estimated from numerical integration. (c) Relationship between the peak $\Delta u_{e,L}$ (black) and $\Delta u_{i,L}$ (blue) jet velocities and λ_C estimated from numerical integration. Since each turbulence interval is characterized by a single λ_C, all reconnection events within a given interval are associated with the same value of λ_C. In panels (a) and (c), the electron jet speeds associated with the ion jets are highlighted in red.

C. Relationship with the Magnetic Correlation Length

Figures 7b,c examine the dependence of the reconnecting current sheet properties on λ_C. Since λ_C is an average quantity for each interval, a distribution of thicknesses and jet speeds is present at each λ_C. For any given turbulent environment, there will be a distribution of different current sheet lengths, which will likely depend on λ_C and, therefore, a change in the distribution of current sheet properties as a function of λ_C is expected if electron-only reconnection is more prevalent for small λ_C.

From Figure 7b, current sheet thicknesses appear to be centered around $\sim d_i$ for λ_C larger than a few tens of d_i, while, for shorter λ_C, the distribution shifts to include more thin sub-proton-scale reconnection events. Similar behaviour is found for the peak electron jet speeds in Figure 7c, where the distribution appears to be roughly constant and centered around several times $\Delta V_{A,L}$ at large λ_C, while at short λ_C there is a slight shift toward faster jets. The peak ion jet speeds are also displayed in Figure 7c, but a clear trend with λ_C is not apparent. Ion-coupled events are identified in intervals across the full range of λ_C. However, since λ_C provides an average size of magnetic structures in a turbulent environment, it is possible for ion-coupled reconnection to be present at individual current sheets even for small λ_C. It is the overall prevalence of such ion-coupled reconnection that is expected to change with λ_C, which is difficult to ascertain due to the limited number of ion-coupled events identified in the present study. Identifying further ion-coupled reconnection events in future studies would help to reveal if any statistical trend is present.

The relationship between λ_C and the reconnection properties is further examined by dividing the events into two sub-sets, those with $\lambda_C < 21.4d_i$ and those with $\lambda_C > 21.4d_i$, where $21.4d_i$ is the median λ_C. Cumulative distributions for the current sheet thicknesses and peak electron jet speeds are computed for each subset in Figure 8a and Figure 9a, respectively. In both cases, differences in the cumulative distributions are present between the two subsets with the distribution shifted toward thinner current sheets and faster electron jets for shorter λ_C. Performing a two-sample Kolmogorov-Smirnov test[126], which estimates the significance of the difference between two empirical cumulative distribution functions in a manner that is independent of the underlying distributions for the samples, indicates the two subsets are drawn from different underlaying distributions with 99.7% confidence for the current sheet thickness and 90% confidence for the electron jet speeds.

A potential bias can be introduced into the distributions due to the finite time resolution of the measurements, since it will not be possible to observe a reconnecting current sheet below a particular thickness for larger $\langle u_{i,N} \rangle_{10d_i}$ and a fixed measurement cadence. To examine the impact of this bias, Figure 8b and Figure 9b show the same analysis of the cumulative distributions, but limiting it to reconnection events where $\langle u_{i,N} \rangle_{10d_i} < 250$ km/s and the current sheet thickness $>$ (250 km/s) $\times$ (0.06 s) based on twice the temporal resolution of the electron measurements. These criteria limit the analysis such that all permitted current sheet thicknesses are observable at any $\langle u_{i,N} \rangle_{10d_i}$ in the dataset if a given reconnection event were of that thickness. Using these additional criteria, the distributions of current sheet thicknesses continue to show a clear shift toward thinner reconnection event for smaller λ_C, with 94% confidence that two subsets are drawn from different underlaying distributions. For the electron jet speeds, the two subsets are less distinct with 62% confidence that the events are drawn from different underlaying distributions. A difference is present in the tails of the electron jet speed distributions, with smaller λ_C having slightly less low speed jets and slightly more high speed jets, which may be notable given that the Kolmogorov-Smirnov test is most sensitive to differences in the core of the distribution[126]. However, more events would be needed to clarify if the statistics in the tails of the distributions are significant.

VII. DISCUSSION

A. Electron-Only Reconnection and the Effective Reynolds Number in Collisionless Plasmas

We find that λ_C systematically varies from $\sim 10d_i$ to $\sim 100d_i$ between the sub-solar magnetosheath and the flanks. This range places magnetosheath turbulence in the ideal parameter regime for electron-only reconnection to occur based on numerical experiments, which likely explains why such events appear to be prevalent in the magnetosheath. A minority of partially or fully ion-coupled reconnection events are also present across the range of λ_C and a number of factors could contribute to the presence of such events. Even within environments with very short correlation lengths, it is still possible for some current sheets in the ensemble of magnetic structures generated by the turbulence to have long enough length scales for ions to couple into the reconnected field lines and form ions jets. It is also known

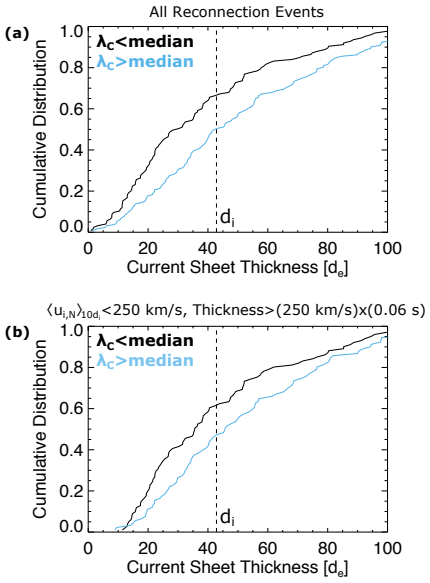

FIG. 8. Cumulative distribution functions for the thickness of the reconnecting current sheets with (a) showing all observed reconnection events and (b) showing only reconnection events for which $\langle u_{i,N}\rangle_{10d_i} < 250$ km/s and the current sheet thickness is greater than (250 km/s) $\times$ (0.06 s), which ensures any current sheet thickness in the sample can be resolved by the FPI measurements at any advection velocity in the sample and mitigates the possible bias introduced by thin fast moving current sheets being unresolvable at a given measurement resolution. Cumulative distributions for reconnection events within intervals with λ_C less than the median value ($21.4d_i$) are shown in black and events within intervals with λ_C greater than the median value are shown in blue.

that large-scale current sheets, which have their origin in the solar wind, can be advected through the bow shock and undergo magnetic reconnection[116,127]. While it is not obvious that the reconnection events examined in this study are such solar wind origin current sheets, it is possible that such current sheets are embedded within the turbulent fluctuations and may, in fact, play a role in the turbulent dynamics of the magnetosheath. Furthermore, the fact that λ_C increases toward the flanks suggests fully ion-coupled reconnection will become more prevalent further down the flanks. A larger sample of such ion-coupled magnetic reconnection is needed to further explore these possibilities; however, the present study

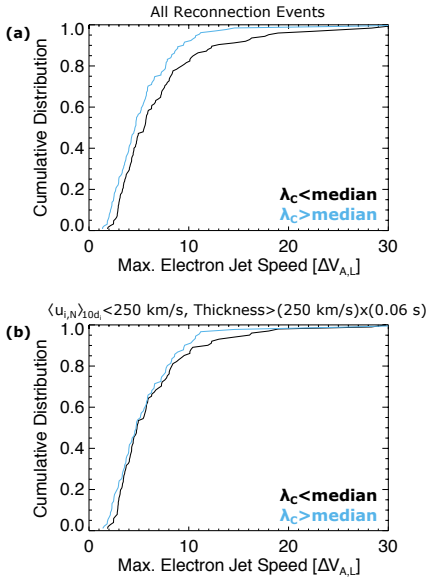

FIG. 9. Cumulative distribution functions for the peak $\Delta u_{e,L}$ in units of $\Delta V_{A,L}$ examined in the same manner as Figure 8, with (a) showing all of the reconnection events and (b) showing only reconnection events for which $\langle u_{i,N} \rangle_{10d_i} < 250$ km/s and the current sheet thickness is greater than (250 km/s) $\times$ (0.06 s). Cumulative distributions for reconnection events within intervals with λ_C less than the median value ($21.4d_i$) are shown in black and events within intervals with λ_C greater than the median value are shown in blue.

indicates such events are present in the magnetosheath at the thicker ion-scale current sheets.

The magnetic correlation length provides an average size for the ensemble of magnetic structures that form the turbulence. However, λ_C is weighted toward the size of the largest structures, since most of the fluctuation energy is contained in the largest scales for typical turbulent dynamics. Therefore, λ_C can be interpreted as being related to the driving scale of the turbulence. As such, the quantity $(\lambda_C/d_i)^{4/3}$ can be used as a proxy for the effective Reynolds number in collisionless plasmas[112] in analogy with collisional systems where the Reynolds number can be similarly related to the scale separation between λ_C and the scale at which dissipation is expected to dominate over the nonlinear dynamics, often referred to

as the Kolmogorov dissipation scale. The analogy is based on the fact that dissipation in collisionless systems is expected to occur through the multitude of kinetic processes that likely come into play at scales smaller than the ion length scales. For the range of λ_C found in Figure 3, the effective Reynolds number ranges from $\sim$ 16 to 1524. While this effective Reynolds number may be reasonable for high Reynolds number systems where the scale separation between λ_C and d_i is much larger than the scale separation between the largest relevant ion scales and the electron scales, the relationship is likely more complex as λ_C approaches the ion scales since many processes can contribute to collisionless dissipation from ion through electron scales and the behaviour and relative importance can depended on a variety of parameters, such as the amplitude of the fluctuations at ion scales or the plasma β, for example. As a result, collisionless dissipation may or may not be significant relative to the nonlinear dynamics at d_i.

The results show that as λ_C approaches a few tens of d_i, the nature of turbulence-driven reconnection can fundamentally change, such that reconnecting current sheets tend to be thinner and may undergo electron-only reconnection. One might, therefore, expect electron-only reconnection to be relevant for collisionless plasmas with relatively low Reynolds numbers. However, it is notable that reconnection dynamics appear to shift toward electron scales in the small λ_C regime, which may suggest shorter length scales comparable to d_e are more appropriate to associate with the effective Reynolds number in these situations. Even if reconnection itself is not contributing significantly to energy dissipation directly, the presence of electron-only reconnection suggests nonlinear dynamics continue to be active at sub-proton scales, again motivating an adjustment to the effective length scale associated with energy dissipation in the collisionless regime. Nevertheless, the results imply that, unlike collisional turbulence, in which resistivity and/or viscosity are always responsible for energy dissipation, in collisionless plasmas, the driving scale of the turbulence or equivalently the effective Reynolds number can alter the nature of energy dissipation.

One might also expect that in turbulent plasmas with large λ_C or equivalently large effective Reynolds numbers, such as the solar wind where λ_C can be many orders of magnitude larger than d_i, the typical length of current sheets will be much larger than d_i and reconnection will primarily be ion-coupled. Larger correlation lengths may contribute to the prevalence of ion-coupled reconnection identified at ion scale currents sheets in the solar wind[41,77]. However, it is also possible that as the effective Reynolds number is increased to

extreme values, additional fluid-scale instabilities resulting from the enhanced nonlinearity may lead to more complex magnetic topologies and electron-only reconnection events could become important again. Magnetohydrodynamic turbulence simulations, particularly in 3D, have demonstrated that as the Reynolds number is increased, what were originally sheet-like current structures at lower Reynolds numbers can become rolled-up, folded, or undulated due to fluid instabilities, such as turbulence-driven Kelvin-Helmholtz instabilities[68,128,129]. This 3D structure may act to effectively limit the length of the reconnection outflows leading to electron-only reconnection, although further numerical work examining the impact of complex current sheet geometries on the behavior of magnetic reconnection either in an idealized or fully turbulent setting is required to explore this possibility. Additionally, secondary magnetic reconnection associated with the instability, "burstiness", or interaction of larger ion-coupled reconnection jets in turbulent plasmas with large λ_C may also create conditions favourable for electron-only reconnection[62,130]. Detailed examination of small-scale current sheets for possible evidence of electron-only reconnection with current missions or, ideally, future missions[131] capable of resolving electron and/or ion flows down to the electron scales in plasma environments, such as the solar wind, which have much larger correlation lengths will help to extend the results of the present study.

B. The Role of Reconnection in Turbulent Dissipation

The present study demonstrates that small-scale magnetic reconnection events are a common feature in the turbulent magnetosheath, occurring at $\sim 10\%$ of intense current sheets. An open question is the extent to which these reconnection events contribute to the dissipation of turbulence. The fraction of the turbulent energy dissipation rate associated with magnetic reconnection, ϵ_{rec}, in units of energy per unit mass per unit time can be estimated as (c.f., Ref. 132)

$$\epsilon_{rec} \approx N_{rec} f_{rec} \left(\alpha_i + \alpha_e\right) V_{A,inflow}^2 \left(\frac{V_{A,inflow}}{\lambda_C}\mathcal{R}\right), \tag{8}$$

where N_{rec} is the number of reconnection events in the turbulent volume and f_{rec} is the fraction of particles in the turbulent volume that interact with a typical reconnection event over its lifetime, such that $N_{rec}f_{rec}$ is the fraction of particles in the turbulent volume accelerated by reconnection. α_i and α_e are the fraction of the available magnetic energy converted into

ion and electron thermal energy, respectively, and $\mathcal{R}$ is the dimensionless reconnection rate. $V_{A,inflow}^2$ represents the amount of magnetic energy available to be reconnected per unit mass per reconnection event, while $(V_{A,inflow}/\lambda_C)\,\mathcal{R}$ is the timescale over which magnetic reconnection occurs, assuming the size of the reconnection inflow region is comparable to λ_C. If magnetic reconnection were the only process responsible for turbulent dissipation, then ϵ_{rec} would be equal to the energy cascade rate in a statistically steady state.

A number of the quantities in Equation 8 can be estimated from the results of the presents study. Based on the intervals examined, the dimensional part of Equation 8, $V_{A,inflow}^3/\lambda_C$, varies from 2×10^6 m^2/s^3 (10^{th} percentile) to 6×10^8 m^2/s^3 (90^{th} percentile) or, if the mass density of the turbulent intervals is taken into account, 8×10^{-14} W/m^3 to 3×10^{-11} W/m^3 across the 60 intervals. This range extends to values larger than previous estimates of 5×10^6 m^2/s^3 or 10^{-16} to 10^{-12} W/m^3 for the energy cascade rate in the magnetosheath[91,92], as well as estimates of 3×10^{-12} W/m^3 for Landau damping in the turbulent magnetosheath[48]. Therefore, depending on the remaining dimensionless factors in Equation 8, which are presently much more uncertain, magnetic reconnection could at least partially contribute to dissipating magnetosheath turbulence.

The fact that $\sim 10\%$ of current structures with amplitude greater than 3 times the rms $|\mathbf{j}|$ are found to be reconnecting provides some insight into $N_{rec}f_{rec}$. However, additional information is needed about which and/or how many particles are processed by a reconnection event in a turbulent environment and it is also possible that additional reconnection events at smaller amplitude current sheets could contribute as well. $N_{rec}f_{rec}$ can be re-expressed as $n_{rec}N_{acc}/n$ in terms of the number density of reconnection events (n_{rec}), number of particles accelerated by the typical reconnection event (N_{acc}), and the particle number density (n) of the turbulent region. The density of current sheets can be estimated as $\sim \lambda_C^{-3}$ and, if $\sim 10\%$ of those were reconnecting, $n_{rec} \sim 0.1\lambda_C^{-3}$. If only the particles within a current sheet were to be accelerated, the volume of the current sheet can be estimated as $\lambda_C^2\delta$ and $N_{acc} \sim n\lambda_C^2\delta$, where δ is the current sheet thickness. In this scenario, $N_{rec}f_{rec} \sim 0.1\delta/\lambda_C$, which based on the events examined in this study gives $N_{rec}f_{rec} \sim 0.005$. On the other hand, since particles are inflowing into the reconnection event, N_{acc} may be larger. As an upper limit, if the all of the particles in the volume λ_C^3 were to be fed into the reconnection event, this would result in $N_{rec}f_{rec} \sim 0.1$. The above estimates are based on the simplest scenario where reconnection events occur at the interface of correlation length magnetic structures

and have lengths comparable to λ_C[9,78,132]; however, if current sheets were more fragmented due to instabilities, as discussed in Section VII A, estimates could be more complex.

The reconnection rate and fraction of energy converted to heating both require further study to constrain, particularly for electron-only reconnection. For standard ion-coupled reconnection, $\mathcal{R} \sim 0.1$ is often taken as a nominal value. However, laminar studies of 2D electron-only reconnection, show that the reconnection rate can be significantly higher for electron-only reconnection, increasing to values greater than 0.6 depending on the length of the current sheet[78] and $\mathcal{R} \sim 0.25$ has been estimated using MMS observations for a single electron-only reconnection event[133]. In terms of the fraction of energy converted into heating, previous observational studies of magnetopause reconnection have estimated, $\alpha_i \sim (3/2) \times 0.13$ and $\alpha_e \sim (3/2) \times 0.017$ for ion-coupled reconnection, where 3/2 accounts for the conversion between temperature change and internal energy[124,125]. However, the nature and amount of heating in electron-only reconnection remains unclear and one might expect that any heating that does occur would only be imparted to the electrons, although this has yet to be confirmed. Observationally constraining the heating associated with reconnection can be challenging, requiring the identification and characterization of clear temperature changes associated with heating, which is beyond the scope of the present study. Additionally, the profile of heating within a reconnection event may be spatially complex and any heating is likely to occur through collisionless processes that are in principle reversible, adding further complications. It is therefore, expected that the dimensionless factors will decrease ϵ_{rec} relative to $V^3_{A,inflow}/\lambda_C$. Assuming $N_{rec}f_{rec} \sim 0.1$, $\alpha_i + \alpha_e \sim 3/2\,(0.147)$ is equivalent to ion-coupled reconnection but potentially partitioned differently between ions and electrons, and $\mathcal{R} \sim 0.25$, gives ϵ_{rec} in the range $1{\times}10^4$ m^2/s^3 to $3{\times}10^6$ m^2/s^3 across the 60 intervals examined in this study, which is a reasonable range to be relevant to the turbulent cascade in the magnetosheath, potentially alongside or synergistically with other types of coherent structures, such as electron vortices[134], and processes, such as Laundau damping[48]. However, given the uncertainty in some of the dimensionless parameters, significantly more study using both numerical simulations and detailed spacecraft observations are needed to constrain the quantities outlined above.

The above estimates are based on the observed amount of energy that is available to reconnect, which, in conjunction with the outlined assumptions about the structure of the reconnection events and how energy is partitioned between thermal and other forms of en-

ergy, provides an estimate for the total amount of energy dissipation that is facilitated by the reconnection process either at the reconnection site or through secondary processes excited in the coherent reconnection outflow region. These estimates are somewhat distinct in perspective, but perhaps complimentary, to recent estimates of the energy dissipation associated with magnetic reconnection inferred from the locally observed $\mathbf{J} \cdot \mathbf{E}'$ in one interval of magnetosheath turbulence that seem to suggest that reconnection makes a minor contribution to dissipation[135]. The apparent discrepancy may be associated with variability across magnetosheath intervals, as is apparent in the range of values in the estimates above, or could potentially be cause by spatially nonuniform dissipation across the entire reconnection outflow region, which may be challenging to infer from only a limited number of reconnection events encountered in a given interval.

C. The Variation of the Magnetosheath Correlation Length

A final interesting topic is the origin of the systematic variation of λ_C across the magnetosheath. Previous statistical studies of energy spectra in the magnetosheath[97] have suggested that the bow shock generates a broadband distribution of random fluctuations with a shallower power law than fully developed turbulence, which evolve through nonlinear interactions as the plasma is advected away from the bow shock to form a more fully-developed Kolmogorov-like spectrum in the flanks. As the nonlinear interactions redistribute the energy into a steeper power law, starting from the more quickly evolving small-scales and progressing to the large scales, an increase in λ_C could occur with time. In this scenario, electron-only reconnection might be viewed as a transient phenomenon, which occurs when turbulence is initially developing from a broadband distribution of random fluctuations. On the other hand, the plasma observed in the flanks may not have advected from the sub-solar point, but instead could have passed through the flanks of the bow shock. In this case, differences in how the shock processes solar wind turbulence and generates new fluctuations under different geometries may have an influence on λ_C. Transient phenomena (e.g., magnetosheath jets near the sub-solar point[136]) and instabilities (e.g., temperature anisotropy instabilities in the magnetosheath or the Kelvin-Helmholtz instability on the flanks of the magnetopause[137]) may also play a role in driving the turbulent fluctuations in different regions of the magnetosheath and, thus, influence λ_C. Examining these possibilities will

require a deeper understanding of the generation and interaction of turbulence with collisionless shocks, as well as a more detailed examination of the evolution of turbulence in the magnetosheath over large spatial and temporal scales, ideally with simultaneous multi-point measurements.

VIII. CONCLUSIONS

Motivated by recent observations of small-scale turbulence-driven magnetic reconnection in Earth's magnetosheath that appears to be undergoing a novel form of electron-only magnetic reconnection, we perform a systematic examination of magnetic reconnection in the turbulent magnetosheath, which has been enabled by the uniquely high-resolution measurements provided by MMS. The aim of the study is to explore how prevalent magnetic reconnection is in turbulent plasmas and how the properties of the reconnection depends on the magnetic correlation length of the turbulence. Reconnection events are identified using a partially automated method, in which intense current structures with peak amplitudes greater than three times the rms current are searched for magnetic field profiles and electron flow perturbations that are potentially consistent with quasi-2D guide field reconnection and the candidate events are then manually verified. Based on this analysis, small-scale reconnection events appear to be a relatively common feature in magnetosheath turbulence, with 256 reconnection events identified that are distributed across all but six of the analyzed turbulence intervals, corresponding to $\sim 10\%$ of intense current sheets having clear evidence of magnetic reconnection.

The majority of events have super-Alfvénic electron jets with no clear evidence of ion jets, potentially consistent with electron-only reconnection or with encountering the events within the IDR. However, a subset of 18 events are identified with clear ion jets based on an analysis of the Walén relationship. When examining the thickness of the reconnecting current sheets, faster electron jet speeds tend to occur at thinner sub-ion-scale current sheets that are not clearly embedded within an ion-scale current sheet, again consistent with the expectations for electron-only reconnection, while ion jet signatures are identified almost exclusively at the thicker ion-scale current sheets. The relatively high occurrence of reconnection events without ion jets compared to those with ion jets, despite the ion jets in standard ion-coupled reconnection occupying a larger volume of space than the IDR, also suggests electron-only

reconnection is occurring.

The correlation length is found to systematically vary between the sub-solar magnetosheath and the flanks with values increasing from $\sim 10d_i$ to several tens or even hundreds of d_i in a manner. This trend is apparent even when restricting the examination to a particular range of θ_{UB}, suggesting that it is not simply an artefact of anisotropy in the correlation function in conjunction with different flow directions relative to the background magnetic field in different regions of the magnetosheath and, instead, may be due to a systematic change in the overall size of the large-scale fluctuations. Since the magnetic correlation length is expected to correspond with the typical size of the large-scale magnetic structures in a turbulent environment, it will constrain the typical length of current sheets formed by the turbulent fluctuations. The range of correlation lengths is consistent with the range of current sheet lengths over which the transition from ion-coupled to electron-only reconnection is expected to occur based on numerical simulations. A tendency for a greater proportion of reconnection events occurring at thin sub-ion-scale current sheets with potentially faster electron jets is observed for correlation lengths around $10d_i$ to $20d_i$. An obvious dependence of the ion jet speed on the correlation length is not observed, likely due to the small number of events with clear ion jets in the present study. However, the behavior of the electron jets and current sheet thicknesses with λ_C appears to be consistent with electron-only reconnection becoming more prevalent as λ_C gets shorter, in accordance with expectations from laminar and turbulent numerical simulations.

The results provide observational evidence that the correlation length of the turbulence can impact the nature of turbulence-driven reconnection, thus influencing the small-scale nonlinear dynamics and dissipation of the turbulent fluctuations. The dataset compiled through this work will likely be useful for directly comparing with turbulence simulations containing magnetic reconnection, such as those performed in Refs. 67 and 82. However, importantly further work needs to be done to explore how to connect diagnostics associated with the global configuration of a turbulent current sheet that can be extracted from a numerical simulation to the more local current sheet diagnostics that can be extracted from the 1D spacecraft trajectories through an event[138]. Future theoretical, numerical, and observational work should be done to characterize the reconnection rate and heating properties, particularly for electron-only reconnection, as well as explore the influence of substructure within the reconnection events, such as temperature anisotropy instabilities[139] or secondary

processes in the outflow region, on the heating and reconnection dynamics under different guide fields and through the transition from ion-coupled to electron-only reconnection. The identification of ion-coupled reconnection events within the magnetosheath, potentially further down the flanks, will help to explore how the presence and speed of ion jets may depend on the correlation length in a statistical manner. Looking for evidence of turbulence-driven reconnection in other solar system plasmas, particularly those with much longer correlation lengths than the magnetosheath, such as the solar wind, with high-resolution measurements capable of resolving scales approaching the electron scales, will help to explore whether electron-only reconnection also becomes relevant at very large effective Reynolds numbers due to additional instabilities. Turbulent plasmas also have the potential to generate complex 3D current structures. While the present analysis focuses on events that appear consistent with quasi-2D guide field reconnection over the scale they are traversed by the spacecraft, continued work should be done to explore more general methods of identifying more complex reconnection events in turbulent plasmas, as has begun to be explored in numerical simulations[69,140]. The examination of other types of current and magnetic field structures within the turbulent magnetosheath that may be associated with magnetic reconnection, in particular small-scale flux ropes that may be linked to the plasmoid instability, should be explored and will help to make contact with theories of how the disruption of current sheets by reconnection may influence the nonlinear dynamics of the turbulence.

SUPPLEMENTAL MATERIALS

See supplemental material for CSV files containing the times and properties of all of the magnetosheath turbulence intervals and reconnection events examined in this study. 'TurbulenceIntervals.csv' provides the UTC start and end times for all 60 intervals in the format "YYYY-MM-DD/hh:mm:ss", the average position of MMS in GSE coordinates, $|\mathbf{U}_0|$, δu_{rms}, $|\mathbf{B}_0|$, δb_{rms}, n_0, T_{i0}, T_{e0}, β_i, β_e, θ_{UB}, $V_{A,0}$, ρ_i, d_i, ρ_e, d_e, and λ_C for the entire interval based on numerical integration. 'ReconnectionEvents.csv' provides the UTC start and end times of the reconnecting current sheets, Δt_{CS}, the peak $|\mathbf{j}|$, θ_{shear} in degrees, current sheet thickness in units of d_e, the local value of d_e, $|\Delta u_{e,L}|/|\Delta V_{A,L}|$, $|\Delta u_{i,L}|/|\Delta V_{A,L}|$, $|\Delta V_{A,L}|$, and $V_{L,inflow}$ as observed by each of the four spacecraft. $\hat{\mathbf{L}}$, $\hat{\mathbf{M}}$, $\hat{\mathbf{N}}$ in GSE coordinates and $\langle \mathbf{u}_i \rangle_{10d_i}$ in LMN coordinates for each event is also given. Start and end times of "0000-00-

00/00:00:00.0000" and quantities denoted with "NaN" indicate an event or parameter was not observed by a given spacecraft.

DATA AVAILABILITY STATEMENT

The data used in this study are publicly available through the MMS Science Data Center (https://lasp.colorado.edu/mms/sdc/public/), Refs. 30, 99–105, and were analyzed using the SPEDAS software package for IDL (http://spedas.org/blog/), Ref. 141.

ACKNOWLEDGMENTS

JES is supported by the Royal Society University Research Fellowship URF\R1\201286. JPE is supported by UKRI/STFC grant ST/S000364/1. TDP is supported by NASA grant 80NSSC20K1781 and National Science Foundation (NSF) grant 2024211. ILG is supported by the Royal Society University Research Fellowship URF\R1\191547. MAS is supported by National Science Foundation (NSF) grant AGS-2024198. The French LPP involvement for the SCM instrument is supported by CNES and CNRS. The authors thank the entire MMS team for their work on the mission and the International Team "Unravelling Solar Wind Microphysics in the Inner Heliosphere" supported by the International Space Science Institute for invaluable discussions.

REFERENCES

[1]J. P. Eastwood, T. D. Phan, S. D. Bale, and A. Tjulin, "Observations of Turbulence Generated by Magnetic Reconnection," Phys. Rev. Lett. **102**, 035001 (2009).

[2]Z. Vörös, Y. L. Sasunov, V. S. Semenov, T. V. Zaqarashvili, R. Bruno, and M. Khodachenko, "Reconnection Outflow Generated Turbulence in the Solar Wind," Astrophys. J. Lett. **797**, L10 (2014).

[3]R. E. Ergun, K. A. Goodrich, J. E. Stawarz, L. Andersson, and V. Angelopoulos, "Large-amplitude electric fields associated with bursty bulk flow braking in the Earth's plasma sheet," J. Geophys. Res. **120**, 1832–1844 (2015).

[4]J. E. Stawarz, R. E. Ergun, and K. A. Goodrich, "Generation of high-frequency electric field activity by turbulence in the Earth's magnetotail," J. Geophys. Res. **120**, 1845–1866 (2015).

[5]R. E. Ergun, K. A. Goodrich, F. D. Wilder, N. Ahmadi, J. C. Holmes, S. Eriksson, J. E. Stawarz, R. Nakamura, K. J. Genestreti, M. Hesse, J. L. Burch, R. B. Torbert, T. D. Phan, S. J. Schwartz, J. P. Eastwood, R. J. Strangeway, O. Le Contel, C. T. Russell, M. R. Argall, P. A. Lindqvist, L. J. Chen, P. A. Cassak, B. L. Giles, J. C. Dorelli, D. Gershman, T. W. Leonard, B. Lavraud, A. Retino, W. Matthaeus, and A. Vaivads, "Magnetic Reconnection, Turbulence, and Particle Acceleration: Observations in the Earth's Magnetotail," Geophys. Res. Lett. **45**, 3338–3347 (2018).

[6]R. E. Ergun, N. Ahmadi, L. Kromyda, S. J. Schwartz, A. Chasapis, S. Hoilijoki, F. D. Wilder, J. E. Stawarz, K. A. Goodrich, D. L. Turner, I. J. Cohen, S. T. Bingham, J. C. Holmes, R. Nakamura, F. Pucci, R. B. Torbert, J. L. Burch, P. A. Lindqvist, R. J. Strangeway, O. Le Contel, and B. L. Giles, "Observations of Particle Acceleration in Magnetic Reconnection-driven Turbulence," Astrophys. J. **898**, 154 (2020).

[7]V. Carbone, P. Veltri, and A. Mangeney, "Coherent structure formation and magnetic field line reconnection in magnetohydrodynamic turbulence," Phys. Fluids A **2**, 1487–1496 (1990).

[8]S. Servidio, W. H. Matthaeus, M. A. Shay, P. A. Cassak, and P. Dmitruk, "Magnetic Reconnection in Two-Dimensional Magnetohydrodynamic Turbulence," Phys. Rev. Lett. **102**, 115003 (2009).

[9]T. D. Phan, J. P. Eastwood, M. A. Shay, J. F. Drake, B. U. Ö. Sonnerup, M. Fujimoto, P. A. Cassak, M. Øieroset, J. L. Burch, R. B. Torbert, A. C. Rager, J. C. Dorelli, D. J. Gershman, C. Pollock, P. S. Pyakurel, C. C. Haggerty, Y. Khotyaintsev, B. Lavraud, Y. Saito, M. Oka, R. E. Ergun, A. Retino, O. Le Contel, M. R. Argall, B. L. Giles, T. E. Moore, F. D. Wilder, R. J. Strangeway, C. T. Russell, P. A. Lindqvist, and W. Magnes, "Electron magnetic reconnection without ion coupling in Earth's turbulent magnetosheath," Nature **557**, 202–206 (2018).

[10]J. E. Stawarz, J. P. Eastwood, T. D. Phan, I. L. Gingell, M. A. Shay, J. L. Burch, R. E. Ergun, B. L. Giles, D. J. Gershman, O. Le Contel, P. A. Lindqvist, C. T. Russell, R. J. Strangeway, R. B. Torbert, M. R. Argall, D. Fischer, W. Magnes, and L. Franci, "Properties of the Turbulence Associated with Electron-only Magnetic Reconnection in

Earth's Magnetosheath," Astrophys. J. Lett. **877**, L37 (2019).

[11]W. H. Matthaeus and S. L. Lamkin, "Turbulent magnetic reconnection," Phys. Fluids **29**, 2513–2534 (1986).

[12]A. Lazarian, G. Eyink, E. Vishniac, and G. Kowal, "Turbulent reconnection and its implications," Phil. Trans. R. Soc. A **373**, 20140144–20140144 (2015).

[13]T. K. M. Nakamura, H. Hasegawa, K. J. Genestreti, R. E. Denton, T. D. Phan, J. E. Stawarz, R. Nakamura, and W. D. Nystrom, "Fast Cross-Scale Energy Transfer During Turbulent Magnetic Reconnection," Geophys. Res. Lett. **48**, e93524 (2021).

[14]S. R. Cranmer, M. Asgari-Targhi, M. P. Miralles, J. C. Raymond, L. Strachan, H. Tian, and L. N. Woolsey, "The role of turbulence in coronal heating and solar wind expansion," Phil. Trans. R. Soc. A **373**, 20140148–20140148 (2015).

[15]P. Wu, "Chromospheric UV Bursts and Turbulent-driven Magnetic Reconnection," Astrophys. J. **885**, 158 (2019).

[16]R. Bruno and V. Carbone, "The Solar Wind as a Turbulence Laboratory," Living Rev. Sol. Phys. **10**, 2 (2013).

[17]M. L. Goldstein, R. T. Wicks, S. Perri, and F. Sahraoui, "Kinetic scale turbulence and dissipation in the solar wind: key observational results and future outlook," Phil. Trans. R. Soc. A **373**, 20140147 (2015).

[18]C. H. K. Chen, S. D. Bale, J. W. Bonnell, D. Borovikov, T. A. Bowen, D. Burgess, A. W. Case, B. D. G. Chandran, T. D. de Wit, K. Goetz, P. R. Harvey, J. C. Kasper, K. G. Klein, K. E. Korreck, D. Larson, R. Livi, R. J. MacDowall, D. M. Malaspina, A. Mallet, M. D. McManus, M. Moncuquet, M. Pulupa, M. L. Stevens, and P. Whittlesey, "The Evolution and Role of Solar Wind Turbulence in the Inner Heliosphere," Astrophys. J. Supp. **246**, 53 (2020).

[19]D. Telloni, L. Sorriso-Valvo, L. D. Woodham, O. Panasenco, M. Velli, F. Carbone, G. P. Zank, R. Bruno, D. Perrone, M. Nakanotani, C. Shi, R. D'Amicis, R. De Marco, V. K. Jagarlamudi, K. Steinvall, R. Marino, L. Adhikari, L. Zhao, H. Liang, A. Tenerani, R. Laker, T. S. Horbury, S. D. Bale, M. Pulupa, D. M. Malaspina, R. J. MacDowall, K. Goetz, T. D. de Wit, P. R. Harvey, J. C. Kasper, K. E. Korreck, D. Larson, A. W. Case, M. L. Stevens, P. Whittlesey, R. Livi, C. J. Owen, S. Livi, P. Louarn, E. Antonucci, M. Romoli, H. O'Brien, V. Evans, and V. Angelini, "Evolution of Solar Wind Turbulence from 0.1 to 1 au during the First Parker Solar Probe-Solar Orbiter Radial Alignment," Astrophys.

J. Lett. **912**, L21 (2021).

[20]J. M. Weygand, M. G. Kivelson, K. K. Khurana, H. K. Schwarzl, S. M. Thompson, R. L. McPherron, A. Balogh, L. M. Kistler, M. L. Goldstein, J. Borovsky, and D. A. Roberts, "Plasma sheet turbulence observed by Cluster II," J. Geophys. Res. **110**, A01205 (2005).

[21]J. Saur, H. Politano, A. Pouquet, and W. H. Matthaeus, "Evidence for weak MHD turbulence in the middle magnetosphere of Jupiter," Astron. Astrophys. **386**, 699–708 (2002).

[22]V. Kaminker, P. A. Delamere, C. S. Ng, T. Dennis, A. Otto, and X. Ma, "Local time dependence of turbulent magnetic fields in Saturn's magnetodisc," Journal of Geophysical Research (Space Physics) **122**, 3972–3984 (2017).

[23]D. Falceta-Gonçalves, G. Kowal, E. Falgarone, and A. C. L. Chian, "Turbulence in the interstellar medium," Nonlin. Proc. Geophys. **21**, 587–604 (2014).

[24]R. Santos-Lima, E. M. de Gouveia Dal Pino, and A. Lazarian, "The Role of Turbulent Magnetic Reconnection in the Formation of Rotationally Supported Protostellar Disks," Astrophys. J. **747**, 21 (2012).

[25]Y. Kawazura, M. Barnes, and A. A. Schekochihin, "Thermal disequilibration of ions and electrons by collisionless plasma turbulence," Proc. Nat. Acad. Sci. **116**, 771–776 (2019).

[26]I. Zhuravleva, E. Churazov, A. A. Schekochihin, S. W. Allen, P. Arévalo, A. C. Fabian, W. R. Forman, J. S. Sanders, A. Simionescu, R. Sunyaev, A. Vikhlinin, and N. Werner, "Turbulent heating in galaxy clusters brightest in X-rays," Nature **515**, 85–87 (2014).

[27]H. Ji, R. Kulsrud, and M. Yamada, "Magnetic Reconnection, Turbulence, and Collisionless Shock," Astrophys. & Space Sci. **298**, 219–226 (2005).

[28]M. R. Brown and D. A. Schaffner, "Laboratory sources of turbulent plasma: a unique MHD plasma wind tunnel," Plasma Sources Science Technology **23**, 063001 (2014).

[29]T. G. White, M. T. Oliver, P. Mabey, M. Kühn-Kauffeldt, A. F. A. Bott, L. N. K. Döhl, A. R. Bell, R. Bingham, R. Clarke, J. Foster, G. Giacinti, P. Graham, R. Heathcote, M. Koenig, Y. Kuramitsu, D. Q. Lamb, J. Meinecke, T. Michel, F. Miniati, M. Notley, B. Reville, D. Ryu, S. Sarkar, Y. Sakawa, M. P. Selwood, J. Squire, R. H. H. Scott, P. Tzeferacos, N. Woolsey, A. A. Schekochihin, and G. Gregori, "Supersonic plasma turbulence in the laboratory," Nature Communications **10**, 1758 (2019).

[30]J. L. Burch, T. E. Moore, R. B. Torbert, and B. L. Giles, "Magnetospheric Multiscale Overview and Science Objectives," Space Sci. Rev. **199**, 5–21 (2016).

[31]J. P. Eastwood, T. D. Phan, J. F. Drake, M. A. Shay, A. L. Borg, B. Lavraud, and M. G. G. T. Taylor, "Energy Partition in Magnetic Reconnection in Earth's Magnetotail," Phys. Rev. Lett. **110**, 225001 (2013).

[32]J. P. Eastwood, M. V. Goldman, T. D. Phan, J. E. Stawarz, P. A. Cassak, J. F. Drake, D. Newman, B. Lavraud, M. A. Shay, R. E. Ergun, J. L. Burch, D. J. Gershman, B. L. Giles, P. A. Lindqvist, R. B. Torbert, R. J. Strangeway, and C. T. Russell, "Energy Flux Densities near the Electron Dissipation Region in Asymmetric Magnetopause Reconnection," Phys. Rev. Lett. **125**, 265102 (2020).

[33]V. M. Vasyliunas, "Theoretical models of magnetic field line merging, 1." Rev. Geophys. Space Phys. **13**, 303–336 (1975).

[34]B. U. O. Sonnerup and B. G. Ledley, "Ogo 5 magnetopause structure and classical reconnection," J. Geophys. Res. **84**, 399–405 (1979).

[35]R. B. Torbert, J. L. Burch, B. L. Giles, D. Gershman, C. J. Pollock, J. Dorelli, L. Avanov, M. R. Argall, J. Shuster, R. J. Strangeway, C. T. Russell, R. E. Ergun, F. D. Wilder, K. Goodrich, H. A. Faith, C. J. Farrugia, P. A. Lindqvist, T. Phan, Y. Khotyaintsev, T. E. Moore, G. Marklund, W. Daughton, W. Magnes, C. A. Kletzing, and S. Bounds, "Estimates of terms in Ohm's law during an encounter with an electron diffusion region," Geophys. Res. Lett. **43**, 5918–5925 (2016).

[36]J. E. Stawarz, L. Matteini, T. N. Parashar, L. Franci, J. P. Eastwood, C. A. Gonzalez, I. L. Gingell, J. L. Burch, R. E. Ergun, N. Ahmadi, B. L. Giles, D. J. Gershman, O. Le Contel, P. A. Lindqvist, C. T. Russell, R. J. Strangeway, and R. B. Torbert, "Comparative Analysis of the Various Generalized Ohm's Law Terms in Magnetosheath Turbulence as Observed by Magnetospheric Multiscale," J. Geophys. Res. **126**, e8447 (2021).

[37]L. Franci, S. S. Cerri, F. Califano, S. Landi, E. Papini, A. Verdini, L. Matteini, F. Jenko, and P. Hellinger, "Magnetic Reconnection as a Driver for a Sub-ion-scale Cascade in Plasma Turbulence," Astrophys. J. Lett. **850**, L16 (2017).

[38]J. W. Dungey, "Interactions of solar plasma with the geomagnetic field," Planetary and Space Sci. **10**, 233–237 (1963).

[39]J. T. Gosling, J. Birn, and M. Hesse, "Three-dimensional magnetic reconnection and the magnetic topology of coronal mass ejection events," Geophys. Res. Lett. **22**, 869–872 (1995).

[40]T. D. Phan, B. Lavraud, J. S. Halekas, M. Øieroset, J. F. Drake, J. P. Eastwood, M. A. Shay, P. S. Pyakurel, S. D. Bale, D. Larson, R. Livi, P. L. Whittlesey, A. Rahmati, M. Pulupa, M. D. McManus, J. L. Verniero, J. W. Bonnell, N. A. Schwadron, M. Stevens, A. W. Case, J. C. Kasper, R. J. MacDowall, P. A. Szabo, A. Koval, K. E. Korreck, T. Dudok de Wit, D. Malaspina, K. Goetz, and P. R. Harvey, "Prevalence of magnetic reconnection in the near-Sun heliospheric current sheet," Astron. & Astrophys. **650**, A13 (2021).

[41]J. T. Gosling, "Observations of Magnetic Reconnection in the Turbulent High-Speed Solar Wind," Astrophys. J. Lett. **671**, L73–L76 (2007).

[42]A. A. Schekochihin, S. C. Cowley, W. Dorland, G. W. Hammett, G. G. Howes, G. G. Plunk, E. Quataert, and T. Tatsuno, "Gyrokinetic turbulence: a nonlinear route to dissipation through phase space," Plasma Physics and Controlled Fusion **50**, 124024 (2008).

[43]B. D. G. Chandran, B. Li, B. N. Rogers, E. Quataert, and K. Germaschewski, "Perpendicular Ion Heating by Low-frequency Alfvén-wave Turbulence in the Solar Wind," Astrophys. J. **720**, 503–515 (2010).

[44]J. M. TenBarge and G. G. Howes, "Current Sheets and Collisionless Damping in Kinetic Plasma Turbulence," Astrophys. J. Lett. **771**, L27 (2013).

[45]S. R. Cranmer, "Ensemble Simulations of Proton Heating in the Solar Wind via Turbulence and Ion Cyclotron Resonance," Astrophys. J. Supp. **213**, 16 (2014).

[46]S. Servidio, A. Chasapis, W. H. Matthaeus, D. Perrone, F. Valentini, T. N. Parashar, P. Veltri, D. Gershman, C. T. Russell, B. Giles, S. A. Fuselier, T. D. Phan, and J. Burch, "Magnetospheric Multiscale Observation of Plasma Velocity-Space Cascade: Hermite Representation and Theory," Phys. Rev. Lett. **119**, 205101 (2017).

[47]S. S. Cerri, M. W. Kunz, and F. Califano, "Dual Phase-space Cascades in 3D Hybrid-Vlasov-Maxwell Turbulence," Astrophys. J. Lett. **856**, L13 (2018).

[48]C. H. K. Chen, K. G. Klein, and G. G. Howes, "Evidence for electron Landau damping in space plasma turbulence," Nature Communications **10**, 740 (2019).

[49]L. Arzamasskiy, M. W. Kunz, B. D. G. Chandran, and E. Quataert, "Hybrid-kinetic Simulations of Ion Heating in Alfvénic Turbulence," Astrophys. J. **879**, 53 (2019).

[50]A. Greco, W. H. Matthaeus, S. Perri, K. T. Osman, S. Servidio, M. Wan, and P. Dmitruk, "Partial Variance of Increments Method in Solar Wind Observations and Plasma Simulations," Space Sci. Rev. **214**, 1 (2018).

[51]D. Perrone, R. Bruno, R. D'Amicis, D. Telloni, R. De Marco, M. Stangalini, S. Perri, O. Pezzi, O. Alexandrova, and S. D. Bale, "Coherent Events at Ion Scales in the Inner Heliosphere: Parker Solar Probe Observations during the First Encounter," Astrophys. J. **905**, 142 (2020).

[52]F. Pecora, S. Servidio, A. Greco, and W. H. Matthaeus, "Identification of coherent structures in space plasmas: the magnetic helicity-PVI method," Astron. & Astrophys. **650**, A20 (2021).

[53]S. S. Cerri and F. Califano, "Reconnection and small-scale fields in 2D-3V hybrid-kinetic driven turbulence simulations," New Journal of Physics **19**, 025007 (2017).

[54]S. Boldyrev and N. F. Loureiro, "Magnetohydrodynamic Turbulence Mediated by Reconnection," The Astrophysical Journal **844**, 125 (2017).

[55]A. Mallet, A. A. Schekochihin, and B. D. G. Chandran, "Disruption of sheet-like structures in Alfvénic turbulence by magnetic reconnection," Monthly Notices of the Royal Astronomical Society **468**, 4862–4871 (2017).

[56]N. F. Loureiro and S. Boldyrev, "Collisionless Reconnection in Magnetohydrodynamic and Kinetic Turbulence," The Astrophysical Journal **850**, 182 (2017).

[57]L. Comisso, Y. M. Huang, M. Lingam, E. Hirvijoki, and A. Bhattacharjee, "Magnetohydrodynamic Turbulence in the Plasmoid-mediated Regime," Astrophys. J. **854**, 103 (2018).

[58]A. Mallet, "The onset of electron-only reconnection," J. Plasma Phys. **86**, 905860301 (2020).

[59]N. F. Loureiro and S. Boldyrev, "Nonlinear Reconnection in Magnetized Turbulence," Astrophys. J. **890**, 55 (2020).

[60]C. C. Haggerty, M. A. Shay, J. F. Drake, T. D. Phan, and C. T. McHugh, "The competition of electron and ion heating during magnetic reconnection," Geophys. Res. Lett. **42**, 9657–9665 (2015).

[61]J. L. Burch, R. B. Torbert, T. D. Phan, L. J. Chen, T. E. Moore, R. E. Ergun, J. P. Eastwood, D. J. Gershman, P. A. Cassak, M. R. Argall, S. Wang, M. Hesse, C. J. Pollock, B. L. Giles, R. Nakamura, B. H. Mauk, S. A. Fuselier, C. T. Russell, R. J. Strangeway, J. F. Drake, M. A. Shay, Y. V. Khotyaintsev, P. A. Lindqvist, G. Marklund, F. D. Wilder, D. T. Young, K. Torkar, J. Goldstein, J. C. Dorelli, L. A. Avanov, M. Oka, D. N. Baker, A. N. Jaynes, K. A. Goodrich, I. J. Cohen, D. L. Turner, J. F. Fennell, J. B. Blake,

J. Clemmons, M. Goldman, D. Newman, S. M. Petrinec, K. J. Trattner, B. Lavraud, P. H. Reiff, W. Baumjohann, W. Magnes, M. Steller, W. Lewis, Y. Saito, V. Coffey, and M. Chandler, "Electron-scale measurements of magnetic reconnection in space," Science **352**, aaf2939 (2016).

[62]R. E. Ergun, K. A. Goodrich, F. D. Wilder, J. C. Holmes, J. E. Stawarz, S. Eriksson, A. P. Sturner, D. M. Malaspina, M. E. Usanova, R. B. Torbert, P. A. Lindqvist, Y. Khotyaintsev, J. L. Burch, R. J. Strangeway, C. T. Russell, C. J. Pollock, B. L. Giles, M. Hesse, L. J. Chen, G. Lapenta, M. V. Goldman, D. L. Newman, S. J. Schwartz, J. P. Eastwood, T. D. Phan, F. S. Mozer, J. Drake, M. A. Shay, P. A. Cassak, R. Nakamura, and G. Marklund, "Magnetospheric Multiscale Satellites Observations of Parallel Electric Fields Associated with Magnetic Reconnection," Phys. Rev. Lett. **116**, 235102 (2016).

[63]F. D. Wilder, R. E. Ergun, J. L. Burch, N. Ahmadi, S. Eriksson, T. D. Phan, K. A. Goodrich, J. Shuster, A. C. Rager, R. B. Torbert, B. L. Giles, R. J. Strangeway, F. Plaschke, W. Magnes, P. A. Lindqvist, and Y. V. Khotyaintsev, "The Role of the Parallel Electric Field in Electron-Scale Dissipation at Reconnecting Currents in the Magnetosheath," J. Geophys. Res. **123**, 6533–6547 (2018).

[64]S. Servidio, W. H. Matthaeus, M. A. Shay, P. Dmitruk, P. A. Cassak, and M. Wan, "Statistics of magnetic reconnection in two-dimensional magnetohydrodynamic turbulence," Phys. Plasmas **17**, 032315 (2010).

[65]S. Donato, S. Servidio, P. Dmitruk, V. Carbone, M. A. Shay, P. A. Cassak, and W. H. Matthaeus, "Reconnection events in two-dimensional Hall magnetohydrodynamic turbulence," Phys. Plasmas **19**, 092307 (2012).

[66]C. T. Haynes, D. Burgess, and E. Camporeale, "Reconnection and Electron Temperature Anisotropy in Sub-proton Scale Plasma Turbulence," Astrophys. J. **783**, 38 (2014).

[67]V. Zhdankin, D. A. Uzdensky, J. C. Perez, and S. Boldyrev, "Statistical Analysis of Current Sheets in Three-dimensional Magnetohydrodynamic Turbulence," Astrophys. J. **771**, 124 (2013).

[68]P. D. Mininni, A. G. Pouquet, and D. C. Montgomery, "Small-Scale Structures in Three-Dimensional Magnetohydrodynamic Turbulence," Phys. Rev. Lett. **97**, 244503 (2006).

[69]J. A. Agudelo Rueda, D. Verscharen, R. T. Wicks, C. J. Owen, G. Nicolaou, A. P. Walsh, I. Zouganelis, K. Germaschewski, and S. Vargas Domínguez, "Three-dimensional magnetic reconnection in particle-in-cell simulations of anisotropic plasma turbulence,"

J. Plasma Phys. **87**, 905870228 (2021).

[70]A. Retinò, D. Sundkvist, A. Vaivads, F. Mozer, M. André, and C. J. Owen, "In situ evidence of magnetic reconnection in turbulent plasma," Nature Phys. **3**, 236–238 (2007).

[71]D. Sundkvist, A. Retinò, A. Vaivads, and S. D. Bale, "Dissipation in Turbulent Plasma due to Reconnection in Thin Current Sheets," Phys. Rev. Lett. **99**, 025004 (2007).

[72]E. Yordanova, Z. Vörös, A. Varsani, D. B. Graham, C. Norgren, Y. V. Khotyaintsev, A. Vaivads, E. Eriksson, R. Nakamura, P.-A. Lindqvist, G. Marklund, R. E. Ergun, W. Magnes, W. Baumjohann, D. Fischer, F. Plaschke, Y. Narita, C. T. Russell, R. J. Strangeway, O. Le Contel, C. Pollock, R. B. Torbert, B. J. Giles, J. L. Burch, L. A. Avanov, J. C. Dorelli, D. J. Gershman, W. R. Paterson, B. Lavraud, and Y. Saito, "Electron scale structures and magnetic reconnection signatures in the turbulent magnetosheath," Geophys. Res. Lett. **43**, 5969–5978 (2016).

[73]Z. Vörös, E. Yordanova, A. Varsani, K. J. Genestreti, Y. V. Khotyaintsev, W. Li, D. B. Graham, C. Norgren, R. Nakamura, Y. Narita, F. Plaschke, W. Magnes, W. Baumjohann, D. Fischer, A. Vaivads, E. Eriksson, P.-A. Lindqvist, G. Marklund, R. E. Ergun, M. Leitner, M. P. Leubner, R. J. Strangeway, O. Le Contel, C. Pollock, B. J. Giles, R. B. Torbert, J. L. Burch, L. A. Avanov, J. C. Dorelli, D. J. Gershman, W. R. Paterson, B. Lavraud, and Y. Saito, "MMS Observation of Magnetic Reconnection in the Turbulent Magnetosheath," J. Geophys. Res. **122**, 11442–11467 (2017).

[74]S. Wang, L.-J. Chen, N. Bessho, M. Hesse, I. Wilson, L. B., B. L. Giles, T. E. Moore, C. T. Russell, R. B. Torbert, and J. L. Burch, "Observational Evidence of Magnetic Reconnection in the Terrestrial Bow Shock Transition Region," Geophys. Res. Lett. **46**, 562–570 (2018).

[75]I. Gingell, S. J. Schwartz, J. P. Eastwood, J. L. Burch, R. E. Ergun, S. Fuselier, D. J. Gershman, B. L. Giles, Y. V. Khotyaintsev, B. Lavraud, P.-A. Lindqvist, W. R. Paterson, T. D. Phan, C. T. Russell, J. E. Stawarz, R. J. Strangeway, R. B. Torbert, and F. Wilder, "Observations of Magnetic Reconnection in the Transition Region of Quasi-Parallel Shocks," Geophys. Res. Lett. **46**, 1177–1184 (2019).

[76]I. Gingell, S. J. Schwartz, J. P. Eastwood, J. E. Stawarz, J. L. Burch, R. E. Ergun, S. A. Fuselier, D. J. Gershman, B. L. Giles, Y. V. Khotyaintsev, B. Lavraud, P. A. Lindqvist, W. R. Paterson, T. D. Phan, C. T. Russell, R. J. Strangeway, R. B. Torbert, and F. Wilder, "Statistics of Reconnecting Current Sheets in the Transition Region of Earth's

Bow Shock," J. Geophys. Res. **125**, e27119 (2020).

[77]R. Mistry, J. P. Eastwood, T. D. Phan, and H. Hietala, "Statistical properties of solar wind reconnection exhausts," J. Geophys. Res. **122**, 5895–5909 (2017).

[78]P. Sharma Pyakurel, M. A. Shay, T. D. Phan, W. H. Matthaeus, J. F. Drake, J. M. TenBarge, C. C. Haggerty, K. G. Klein, P. A. Cassak, T. N. Parashar, M. Swisdak, and A. Chasapis, "Transition from ion-coupled to electron-only reconnection: Basic physics and implications for plasma turbulence," Phys. Plasmas **26**, 082307 (2019).

[79]S. Y. Huang, Q. Y. Xiong, L. F. Song, J. Nan, Z. G. Yuan, K. Jiang, X. H. Deng, and L. Yu, "Electron-only Reconnection in Ion-scale Current Sheet at the Magnetopause," arXiv e-prints , arXiv:2109.13051 (2021).

[80]R. Wang, Q. Lu, S. Lu, C. T. Russell, J. L. Burch, D. J. Gershman, W. Gonzalez, and S. Wang, "Physical Implication of Two Types of Reconnection Electron Diffusion Regions With and Without Ion-Coupling in the Magnetotail Current Sheet," Geophys. Res. Lett. **47**, e88761 (2020).

[81]C. Vega, V. Roytershteyn, G. L. Delzanno, and S. Boldyrev, "Electron-only Reconnection in Kinetic-Alfvén Turbulence," Astrophys. J. Lett. **893**, L10 (2020).

[82]F. Califano, S. S. Cerri, M. Faganello, D. Laveder, M. Sisti, and M. W. Kunz, "Electron-only reconnection in plasma turbulence," Frontiers Phys. **8**, 317 (2020).

[83]G. Arró, F. Califano, and G. Lapenta, "Statistical properties of turbulent fluctuations associated with electron-only magnetic reconnection," Astron. & Astrophys. **642**, A45 (2020).

[84]D. J. Gershman, J. C. Dorelli, A. F. -Viñas, and C. J. Pollock, "The calculation of moment uncertainties from velocity distribution functions with random errors," J. Geophys. Res. **120**, 6633–6645 (2015).

[85]R. Bandyopadhyay, A. Chasapis, R. Chhiber, T. N. Parashar, B. A. Maruca, W. H. Matthaeus, S. J. Schwartz, S. Eriksson, O. Le Contel, H. Breuillard, J. L. Burch, T. E. Moore, C. J. Pollock, B. L. Giles, W. R. Paterson, J. Dorelli, D. J. Gershman, R. B. Torbert, C. T. Russell, and R. J. Strangeway, "Solar Wind Turbulence Studies Using MMS Fast Plasma Investigation Data," Astrophys. J. **866**, 81 (2018).

[86]D. J. Gershman, J. C. Dorelli, L. A. Avanov, U. Gliese, A. Barrie, C. Schiff, D. E. Da Silva, W. R. Paterson, B. L. Giles, and C. J. Pollock, "Systematic Uncertainties in Plasma Parameters Reported by the Fast Plasma Investigation on NASA's Magnetospheric Mul-

tiscale Mission," J. Geophys. Res. **124**, 10,345–10,359 (2019).

[87]O. W. Roberts, R. Nakamura, V. N. Coffey, D. J. Gershman, M. Volwerk, A. Varsani, B. L. Giles, J. C. Dorelli, and C. Pollock, "A Study of the Solar Wind Ion and Electron Measurements From the Magnetospheric Multiscale Mission's Fast Plasma Investigation," J. Geophys. Res. **126**, e29784 (2021).

[88]F. Sahraoui, G. Belmont, L. Rezeau, N. Cornilleau-Wehrlin, J. L. Pinçon, and A. Balogh, "Anisotropic Turbulent Spectra in the Terrestrial Magnetosheath as Seen by the Cluster Spacecraft," Phys. Rev. Lett. **96**, 075002 (2006).

[89]O. Alexandrova, C. Lacombe, and A. Mangeney, "Spectra and anisotropy of magnetic fluctuations in the Earth's magnetosheath: Cluster observations," Annales Geophysicae **26**, 3585–3596 (2008).

[90]S. Y. Huang, F. Sahraoui, X. H. Deng, J. S. He, Z. G. Yuan, M. Zhou, Y. Pang, and H. S. Fu, "Kinetic Turbulence in the Terrestrial Magnetosheath: Cluster Observations," Astrophys. J. Lett. **789**, L28 (2014).

[91]L. Z. Hadid, F. Sahraoui, S. Galtier, and S. Y. Huang, "Compressible Magnetohydrodynamic Turbulence in the Earth's Magnetosheath: Estimation of the Energy Cascade Rate Using in situ Spacecraft Data," Phys. Rev. Lett. **120**, 055102 (2018).

[92]R. Bandyopadhyay, A. Chasapis, R. Chhiber, T. N. Parashar, W. H. Matthaeus, M. A. Shay, B. A. Maruca, J. L. Burch, T. E. Moore, C. J. Pollock, B. L. Giles, W. R. Paterson, J. Dorelli, D. J. Gershman, R. B. Torbert, C. T. Russell, and R. J. Strangeway, "Incompressive Energy Transfer in the Earth's Magnetosheath: Magnetospheric Multiscale Observations," Astrophys. J. **866**, 106 (2018).

[93]L. Matteini, O. Alexandrova, C. H. K. Chen, and C. Lacombe, "Electric and magnetic spectra from MHD to electron scales in the magnetosheath," Mon. Not. R. Astro. Soc. **466**, 945–951 (2017).

[94]X. Zhu, J. He, Y. Wang, and L. Sorriso-Valvo, "Difference of Intermittency between Electric Field and Magnetic Field Fluctuations from Ion Scale Down to Sub-electron Scale in the Magnetosheath Turbulence," Astrophys. J. **893**, 124 (2020).

[95]R. Bandyopadhyay, W. H. Matthaeus, T. N. Parashar, Y. Yang, A. Chasapis, B. L. Giles, D. J. Gershman, C. J. Pollock, C. T. Russell, R. J. Strangeway, R. B. Torbert, T. E. Moore, and J. L. Burch, "Statistics of Kinetic Dissipation in the Earth's Magnetosheath: MMS Observations," Phys. Rev. Lett. **124**, 255101 (2020).

[96]J. He, X. Zhu, D. Verscharen, D. Duan, J. Zhao, and T. Wang, "Spectra of Diffusion, Dispersion, and Dissipation for Kinetic Alfvénic and Compressive Turbulence: Comparison between Kinetic Theory and Measurements from MMS," Astrophys. J. **898**, 43 (2020).

[97]S. Y. Huang, L. Z. Hadid, F. Sahraoui, Z. G. Yuan, and X. H. Deng, "On the Existence of the Kolmogorov Inertial Range in the Terrestrial Magnetosheath Turbulence," Astrophys. J. Lett. **836**, L10 (2017).

[98]H. Li, W. Jiang, C. Wang, D. Verscharen, C. Zeng, C. T. Russell, B. Giles, and J. L. Burch, "Evolution of the Earth's Magnetosheath Turbulence: A Statistical Study Based on MMS Observations," Astrophys. J. Lett. **898**, L43 (2020).

[99]C. T. Russell, B. J. Anderson, W. Baumjohann, K. R. Bromund, D. Dearborn, D. Fischer, G. Le, H. K. Leinweber, D. Leneman, W. Magnes, J. D. Means, M. B. Moldwin, R. Nakamura, D. Pierce, F. Plaschke, K. M. Rowe, J. A. Slavin, R. J. Strangeway, R. Torbert, C. Hagen, I. Jernej, A. Valavanoglou, and I. Richter, "The Magnetospheric Multiscale Magnetometers," Space Sci. Rev. **199**, 189–256 (2016).

[100]O. Le Contel, P. Leroy, A. Roux, C. Coillot, D. Alison, A. Bouabdellah, L. Mirioni, L. Meslier, A. Galic, M. C. Vassal, R. B. Torbert, J. Needell, D. Rau, I. Dors, R. E. Ergun, J. Westfall, D. Summers, J. Wallace, W. Magnes, A. Valavanoglou, G. Olsson, M. Chutter, J. Macri, S. Myers, S. Turco, J. Nolin, D. Bodet, K. Rowe, M. Tanguy, and B. de la Porte, "The Search-Coil Magnetometer for MMS," Space Sci. Rev. **199**, 257–282 (2016).

[101]P.-A. Lindqvist, G. Olsson, R. B. Torbert, B. King, M. Granoff, D. Rau, G. Needell, S. Turco, I. Dors, P. Beckman, J. Macri, C. Frost, J. Salwen, A. Eriksson, L. Åhlén, Y. V. Khotyaintsev, J. Porter, K. Lappalainen, R. E. Ergun, W. Wermeer, and S. Tucker, "The Spin-Plane Double Probe Electric Field Instrument for MMS," Space Sci. Rev. **199**, 137–165 (2016).

[102]R. E. Ergun, S. Tucker, J. Westfall, K. A. Goodrich, D. M. Malaspina, D. Summers, J. Wallace, M. Karlsson, J. Mack, N. Brennan, B. Pyke, P. Withnell, R. Torbert, J. Macri, D. Rau, I. Dors, J. Needell, P.-A. Lindqvist, G. Olsson, and C. M. Cully, "The Axial Double Probe and Fields Signal Processing for the MMS Mission," Space Sci. Rev. **199**, 167–188 (2016).

[103]C. Pollock, T. Moore, A. Jacques, J. Burch, U. Gliese, Y. Saito, T. Omoto, L. Avanov, A. Barrie, V. Coffey, J. Dorelli, D. Gershman, B. Giles, T. Rosnack, C. Salo, S. Yokota,

M. Adrian, C. Aoustin, C. Auletti, S. Aung, V. Bigio, N. Cao, M. Chandler, D. Chornay, K. Christian, G. Clark, G. Collinson, T. Corris, A. De Los Santos, R. Devlin, T. Diaz, T. Dickerson, C. Dickson, A. Diekmann, F. Diggs, C. Duncan, A. Figueroa-Vinas, C. Firman, M. Freeman, N. Galassi, K. Garcia, G. Goodhart, D. Guererro, J. Hageman, J. Hanley, E. Hemminger, M. Holland, M. Hutchins, T. James, W. Jones, S. Kreisler, J. Kujawski, V. Lavu, J. Lobell, E. LeCompte, A. Lukemire, E. MacDonald, A. Mariano, T. Mukai, K. Narayanan, Q. Nguyan, M. Onizuka, W. Paterson, S. Persyn, B. Piepgrass, F. Cheney, A. Rager, T. Raghuram, A. Ramil, L. Reichenthal, H. Rodriguez, J. Rouzaud, A. Rucker, Y. Saito, M. Samara, J.-A. Sauvaud, D. Schuster, M. Shappirio, K. Shelton, D. Sher, D. Smith, K. Smith, S. Smith, D. Steinfeld, R. Szymkiewicz, K. Tanimoto, J. Taylor, C. Tucker, K. Tull, A. Uhl, J. Vloet, P. Walpole, S. Weidner, D. White, G. Winkert, P.-S. Yeh, and M. Zeuch, "Fast Plasma Investigation for Magnetospheric Multiscale," Space Sci. Rev. **199**, 331–406 (2016).

[104]A. C. Rager, J. C. Dorelli, D. J. Gershman, V. Uritsky, L. A. Avanov, R. B. Torbert, J. L. Burch, R. E. Ergun, J. Egedal, C. Schiff, J. R. Shuster, B. L. Giles, W. R. Paterson, C. J. Pollock, R. J. Strangeway, C. T. Russell, B. Lavraud, V. N. Coffey, and Y. Saito, "Electron Crescent Distributions as a Manifestation of Diamagnetic Drift in an Electron-Scale Current Sheet: Magnetospheric Multiscale Observations Using New 7.5 ms Fast Plasma Investigation Moments," Geophys. Res. Lett. **45**, 578–584 (2018).

[105]M. R. Argall, D. Fischer, O. Le Contel, L. Mirioni, R. B. Torbert, I. Dors, M. Chutter, J. Needell, R. Strangeway, W. Magnes, and C. T. Russell, "The Fluxgate-Searchcoil Merged (FSM) Magnetic Field Data Product for MMS," arXiv e-prints , arXiv:1809.07388 (2018).

[106]P. Robert, M. W. Dunlop, A. Roux, and G. Chanteur, "Accuracy of Current Density Determination," ISSI Scientific Reports Series **1**, 395–418 (1998).

[107]G. I. Taylor, "The Spectrum of Turbulence," Proc. R. Soc. A **164**, 476–490 (1938).

[108]A. Chasapis, W. H. Matthaeus, T. N. Parashar, S. A. Fuselier, B. A. Maruca, T. D. Phan, J. L. Burch, T. E. Moore, C. J. Pollock, D. J. Gershman, R. B. Torbert, C. T. Russell, and R. J. Strangeway, "High-resolution Statistics of Solar Wind Turbulence at Kinetic Scales Using the Magnetospheric Multiscale Mission," Astrophys. J. Lett. **844**, L9 (2017).

[109]C. H. K. Chen and S. Boldyrev, "Nature of Kinetic Scale Turbulence in the Earth's Magnetosheath," Astrophys. J. **842**, 122 (2017).

[110]R. Chhiber, A. Chasapis, R. Bandyopadhyay, T. N. Parashar, W. H. Matthaeus, B. A. Maruca, T. E. Moore, J. L. Burch, R. B. Torbert, C. T. Russell, O. Le Contel, M. R. Argall, D. Fischer, L. Mirioni, R. J. Strangeway, C. J. Pollock, B. L. Giles, and D. J. Gershman, "Higher-Order Turbulence Statistics in the Earth's Magnetosheath and the Solar Wind Using Magnetospheric Multiscale Observations," J. Geophys. Res. **123**, 9941–9954 (2018).

[111]J. Cho and E. T. Vishniac, "The Anisotropy of Magnetohydrodynamic Alfvénic Turbulence," Astrophys. J. **539**, 273–282 (2000).

[112]T. N. Parashar, M. Cuesta, and W. H. Matthaeus, "Reynolds Number and Intermittency in the Expanding Solar Wind: Predictions Based on Voyager Observations," Astrophys. J. Lett. **884**, L57 (2019).

[113]J. H. Shue, P. Song, C. T. Russell, J. T. Steinberg, J. K. Chao, G. Zastenker, O. L. Vaisberg, S. Kokubun, H. J. Singer, T. R. Detman, and H. Kawano, "Magnetopause location under extreme solar wind conditions," J. Geophys. Res. **103**, 17691–17700 (1998).

[114]J. T. Gosling and T. D. Phan, "Magnetic Reconnection in the Solar Wind at Current Sheets Associated with Extremely Small Field Shear Angles," Astrophys. J. Lett. **763**, L39 (2013).

[115]H. Tilquin, J. P. Eastwood, and T. D. Phan, "Solar Wind Reconnection Exhausts in the Inner Heliosphere Observed by Helios and Detected via Machine Learning," Astropys. J. **895**, 68 (2020).

[116]J. P. Eastwood, R. Mistry, T. D. Phan, S. J. Schwartz, R. E. Ergun, J. F. Drake, M. Øieroset, J. E. Stawarz, M. V. Goldman, C. Haggerty, M. A. Shay, J. L. Burch, D. J. Gershman, B. L. Giles, P. A. Lindqvist, R. B. Torbert, R. J. Strangeway, and C. T. Russell, "Guide Field Reconnection: Exhaust Structure and Heating," Geophys. Res. Lett. **45**, 4569–4577 (2018).

[117]C. C. Harvey, "Spatial Gradients and the Volumetric Tensor," ISSI Scientific Reports Series **1**, 307–322 (1998).

[118]R. Mistry, J. P. Eastwood, T. D. Phan, and H. Hietala, "Development of bifurcated current sheets in solar wind reconnection exhausts," Geophys. Res. Lett. **42**, 10,513–10,520 (2015).

[119]M. Øieroset, T. D. Phan, J. F. Drake, J. P. Eastwood, S. A. Fuselier, R. J. Strangeway, C. Haggerty, M. A. Shay, M. Oka, S. Wang, L. J. Chen, I. Kacem, B. Lavraud, V. An-

gelopoulos, J. L. Burch, R. B. Torbert, R. E. Ergun, Y. Khotyaintsev, P. A. Lindqvist, D. J. Gershman, B. L. Giles, C. Pollock, T. E. Moore, C. T. Russell, Y. Saito, L. A. Avanov, and W. Paterson, "Reconnection With Magnetic Flux Pileup at the Interface of Converging Jets at the Magnetopause," Geophys. Res. Lett. **46**, 1937–1946 (2019).

[120]M. Swisdak, M. Opher, J. F. Drake, and F. Alouani Bibi, "The Vector Direction of the Interstellar Magnetic Field Outside the Heliosphere," Astrophys. J. **710**, 1769–1775 (2010).

[121]T. D. Phan, G. Paschmann, J. T. Gosling, M. Oieroset, M. Fujimoto, J. F. Drake, and V. Angelopoulos, "The dependence of magnetic reconnection on plasma β and magnetic shear: Evidence from magnetopause observations," Geophys. Res. Lett. **40**, 11–16 (2013).

[122]P. A. Cassak and M. A. Shay, "Scaling of asymmetric magnetic reconnection: General theory and collisional simulations," Phys. Plasmas **14**, 102114 (2007).

[123]M. Swisdak and J. F. Drake, "Orientation of the reconnection X-line," Geophys. Res. Lett. **34**, L11106 (2007).

[124]T. D. Phan, M. A. Shay, J. T. Gosling, M. Fujimoto, J. F. Drake, G. Paschmann, M. Oieroset, J. P. Eastwood, and V. Angelopoulos, "Electron bulk heating in magnetic reconnection at Earth's magnetopause: Dependence on the inflow Alfvén speed and magnetic shear," Geophys. Res. Lett. **40**, 4475–4480 (2013).

[125]T. D. Phan, J. F. Drake, M. A. Shay, J. T. Gosling, G. Paschmann, J. P. Eastwood, M. Oieroset, M. Fujimoto, and V. Angelopoulos, "Ion bulk heating in magnetic reconnection exhausts at Earth's magnetopause: Dependence on the inflow Alfvén speed and magnetic shear angle," Geophys. Res. Lett. **41**, 7002–7010 (2014).

[126]E. D. Feigelson and G. J. Babu, *Modern Statistical Methods for Astronomy* (Cambridge University Press, Cambridge, UK, 2012).

[127]T. D. Phan, G. Paschmann, C. Twitty, F. S. Mozer, J. T. Gosling, J. P. Eastwood, M. Øieroset, H. Rème, and E. A. Lucek, "Evidence for magnetic reconnection initiated in the magnetosheath," Geophys. Res. Lett. **34**, L14104 (2007).

[128]P. D. Mininni and A. Pouquet, "Finite dissipation and intermittency in magnetohydrodynamics," Phys. Rev. E **80**, 025401 (2009).

[129]A. Pouquet, E. Lee, M. E. Brachet, P. D. Mininni, and D. Rosenberg, "The dynamics of unforced turbulence at high Reynolds number for Taylor-Green vortices generalized to MHD," Geophys. & Astrophys. Fluid Dyn. **104**, 115–134 (2010).

[130]M. Zhou, H. Y. Man, X. H. Deng, Y. Pang, Y. Khotyaintsev, G. Lapenta, Y. Y. Yi, Z. H. Zhong, and W. Q. Ma, "Observations of Secondary Magnetic Reconnection in the Turbulent Reconnection Outflow," Geophys. Res. Lett. **48**, e91215 (2021).

[131]D. Verscharen, R. T. Wicks, O. Alexandrova, R. Bruno, D. Burgess, C. H. K. Chen, R. D'Amicis, J. De Keyser, T. D. de Wit, L. Franci, J. He, P. Henri, S. Kasahara, Y. Khotyaintsev, K. G. Klein, B. Lavraud, B. A. Maruca, M. Maksimovic, F. Plaschke, S. Poedts, C. S. Reynolds, O. Roberts, F. Sahraoui, S. Saito, C. S. Salem, J. Saur, S. Servidio, J. E. Stawarz, Š. Štverák, and D. Told, "A Case for Electron-Astrophysics," Experimental Astronomy (2021), 10.1007/s10686-021-09761-5.

[132]M. A. Shay, C. C. Haggerty, W. H. Matthaeus, T. N. Parashar, M. Wan, and P. Wu, "Turbulent heating due to magnetic reconnection," Phys. Plasmas **25**, 012304 (2018).

[133]J. L. Burch, J. M. Webster, M. Hesse, K. J. Genestreti, R. E. Denton, T. D. Phan, H. Hasegawa, P. A. Cassak, R. B. Torbert, B. L. Giles, D. J. Gershman, R. E. Ergun, C. T. Russell, R. J. Strangeway, O. Le Contel, K. R. Pritchard, A. T. Marshall, K. J. Hwang, K. Dokgo, S. A. Fuselier, L. J. Chen, S. Wang, M. Swisdak, J. F. Drake, M. R. Argall, K. J. Trattner, M. Yamada, and G. Paschmann, "Electron Inflow Velocities and Reconnection Rates at Earth's Magnetopause and Magnetosheath," Geophys. Res. Lett. **47**, e89082 (2020).

[134]S. Y. Huang, J. W. Du, F. Sahraoui, Z. G. Yuan, J. S. He, J. S. Zhao, O. Le Contel, H. Breuillard, D. D. Wang, X. D. Yu, X. H. Deng, H. S. Fu, M. Zhou, C. J. Pollock, R. B. Torbert, C. T. Russell, and J. L. Burch, "A statistical study of kinetic-size magnetic holes in turbulent magnetosheath: MMS observations," J. Geophys. Res. **122**, 8577–8588 (2017).

[135]C. Hou, J. He, X. Zhu, and Y. Wang, "Contribution of Magnetic Reconnection Events to Energy Dissipation in Space Plasma Turbulence," Astrophys. J. **908**, 237 (2021).

[136]H. Hietala, T. V. Laitinen, K. Andréeová, R. Vainio, A. Vaivads, M. Palmroth, T. I. Pulkkinen, H. E. J. Koskinen, E. A. Lucek, and H. Rème, "Supermagnetosonic Jets behind a Collisionless Quasiparallel Shock," Phys. Rev. Lett. **103**, 245001 (2009).

[137]J. E. Stawarz, S. Eriksson, F. D. Wilder, R. E. Ergun, S. J. Schwartz, A. Pouquet, J. L. Burch, B. L. Giles, Y. Khotyaintsev, O. Le Contel, P. A. Lindqvist, W. Magnes, C. J. Pollock, C. T. Russell, R. J. Strangeway, R. B. Torbert, L. A. Avanov, J. C. Dorelli, J. P. Eastwood, D. J. Gershman, K. A. Goodrich, D. M. Malaspina, G. T. Marklund,

L. Mirioni, and A. P. Sturner, "Observations of turbulence in a Kelvin-Helmholtz event on 8 September 2015 by the Magnetospheric Multiscale mission," J. Geophys. Res. **121**, 11,021–11,034 (2016).

[138]M. Sisti, S. Fadanelli, S. S. Cerri, M. Faganello, F. Califano, and O. Agullo, "Characterizing current structures in 3D hybrid-kinetic simulations of plasma turbulence," Astron. & Astrophys. **in press** (2021), 10.1051/0004-6361/202141902.

[139]F. Finelli, S. S. Cerri, F. Califano, F. Pucci, D. Laveder, G. Lapenta, and T. Passot, "Bridging hybrid- and full-kinetic models with Landau-fluid electrons. I. 2D magnetic reconnection," Astron. & Astrophys. **653**, A156 (2021).

[140]M. Sisti, F. Finelli, G. Pedrazzi, M. Faganello, F. Califano, and F. Delli Ponti, "Detecting Reconnection Events in Kinetic Vlasov Hybrid Simulations Using Clustering Techniques," Astrophys. J. **908**, 107 (2021).

[141]V. Angelopoulos, P. Cruce, A. Drozdov, E. W. Grimes, N. Hatzigeorgiu, D. A. King, D. Larson, J. W. Lewis, J. M. McTiernan, D. A. Roberts, C. L. Russell, T. Hori, Y. Kasahara, A. Kumamoto, A. Matsuoka, Y. Miyashita, Y. Miyoshi, I. Shinohara, M. Teramoto, J. B. Faden, A. J. Halford, M. McCarthy, R. M. Millan, J. G. Sample, D. M. Smith, L. A. Woodger, A. Masson, A. A. Narock, K. Asamura, T. F. Chang, C. Y. Chiang, Y. Kazama, K. Keika, S. Matsuda, T. Segawa, K. Seki, M. Shoji, S. W. Y. Tam, N. Umemura, B. J. Wang, S. Y. Wang, R. Redmon, J. V. Rodriguez, H. J. Singer, J. Vandegriff, S. Abe, M. Nose, A. Shinbori, Y. M. Tanaka, S. UeNo, L. Andersson, P. Dunn, C. Fowler, J. S. Halekas, T. Hara, Y. Harada, C. O. Lee, R. Lillis, D. L. Mitchell, M. R. Argall, K. Bromund, J. L. Burch, I. J. Cohen, M. Galloy, B. Giles, A. N. Jaynes, O. Le Contel, M. Oka, T. D. Phan, B. M. Walsh, J. Westlake, F. D. Wilder, S. D. Bale, R. Livi, M. Pulupa, P. Whittlesey, A. DeWolfe, B. Harter, E. Lucas, U. Auster, J. W. Bonnell, C. M. Cully, E. Donovan, R. E. Ergun, H. U. Frey, B. Jackel, A. Keiling, H. Korth, J. P. McFadden, Y. Nishimura, F. Plaschke, P. Robert, D. L. Turner, J. M. Weygand, R. M. Candey, R. C. Johnson, T. Kovalick, M. H. Liu, R. E. McGuire, A. Breneman, K. Kersten, and P. Schroeder, "The Space Physics Environment Data Analysis System (SPEDAS)," Space Sci. Rev. **215**, 9 (2019).

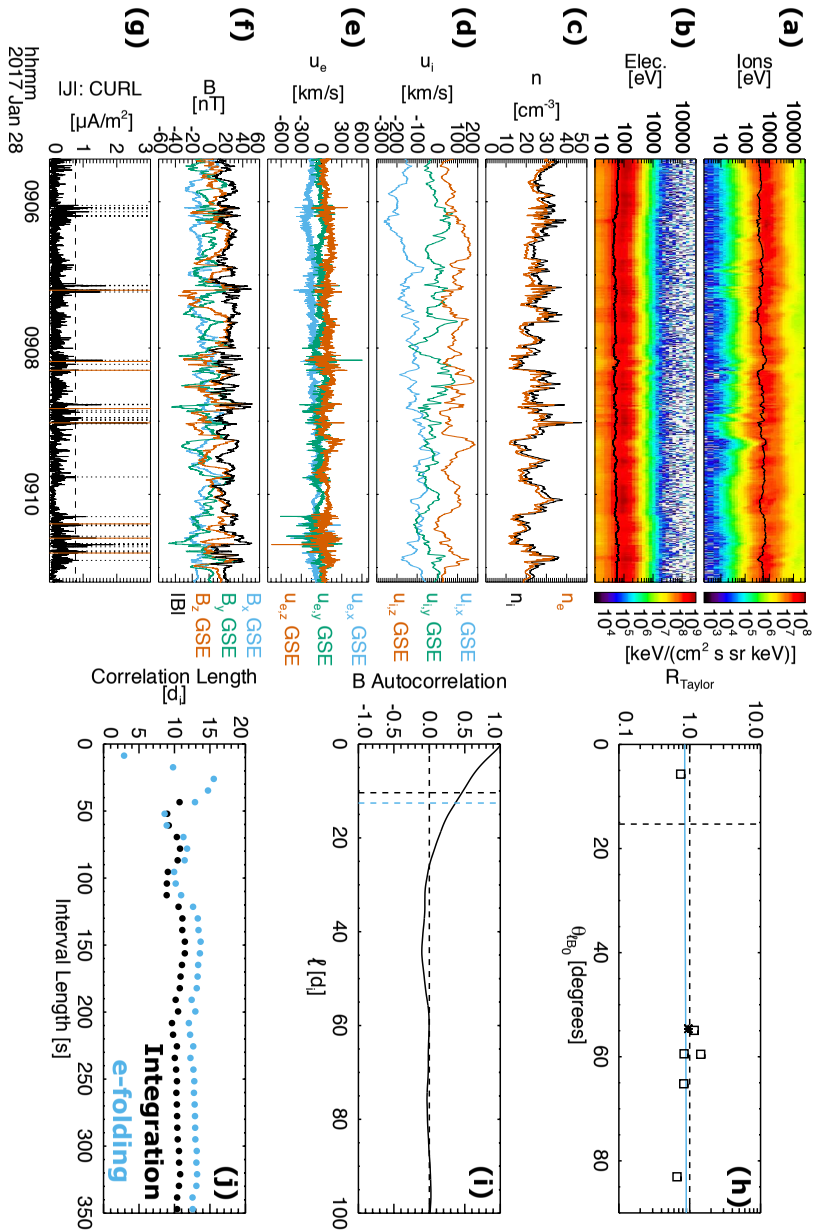

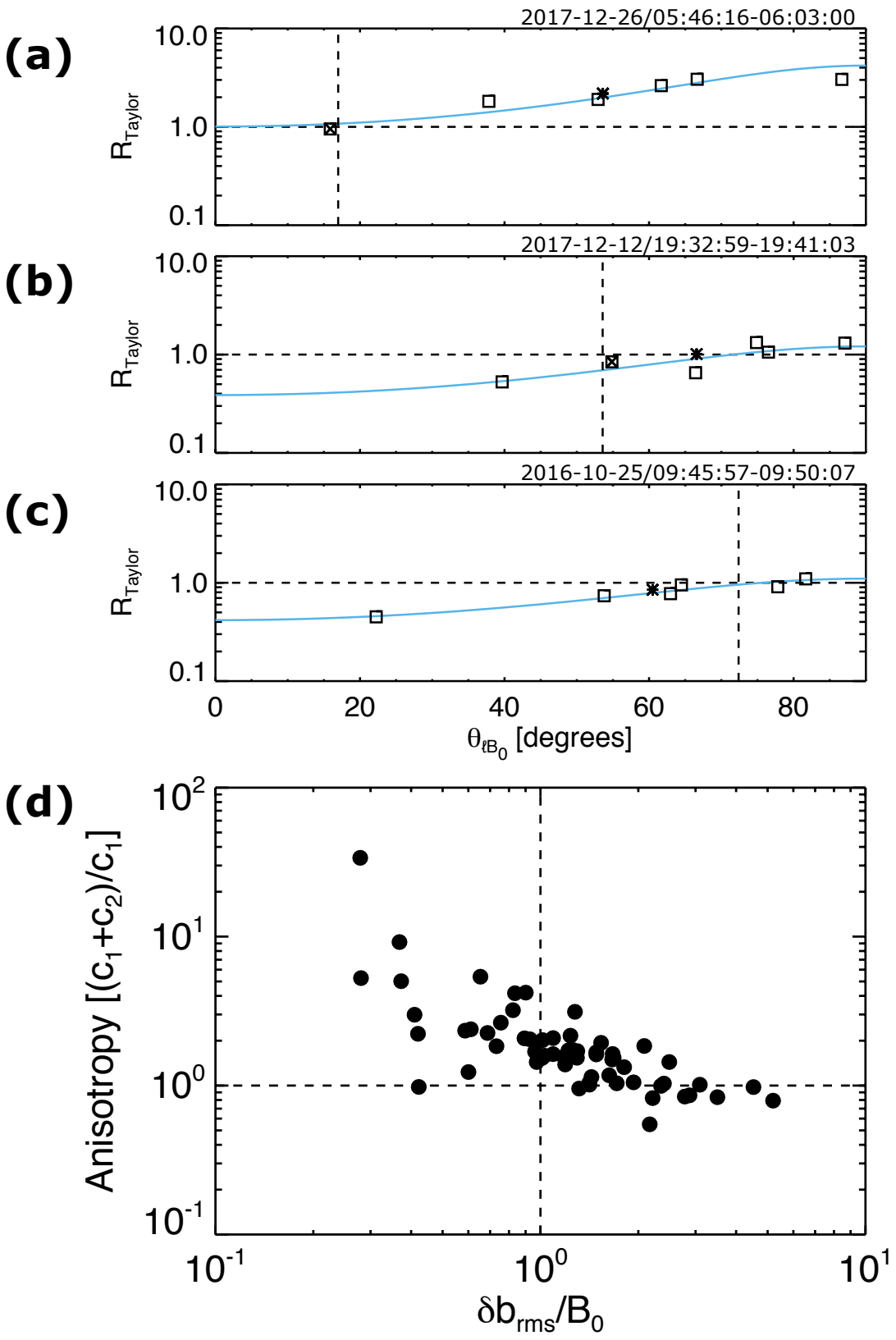

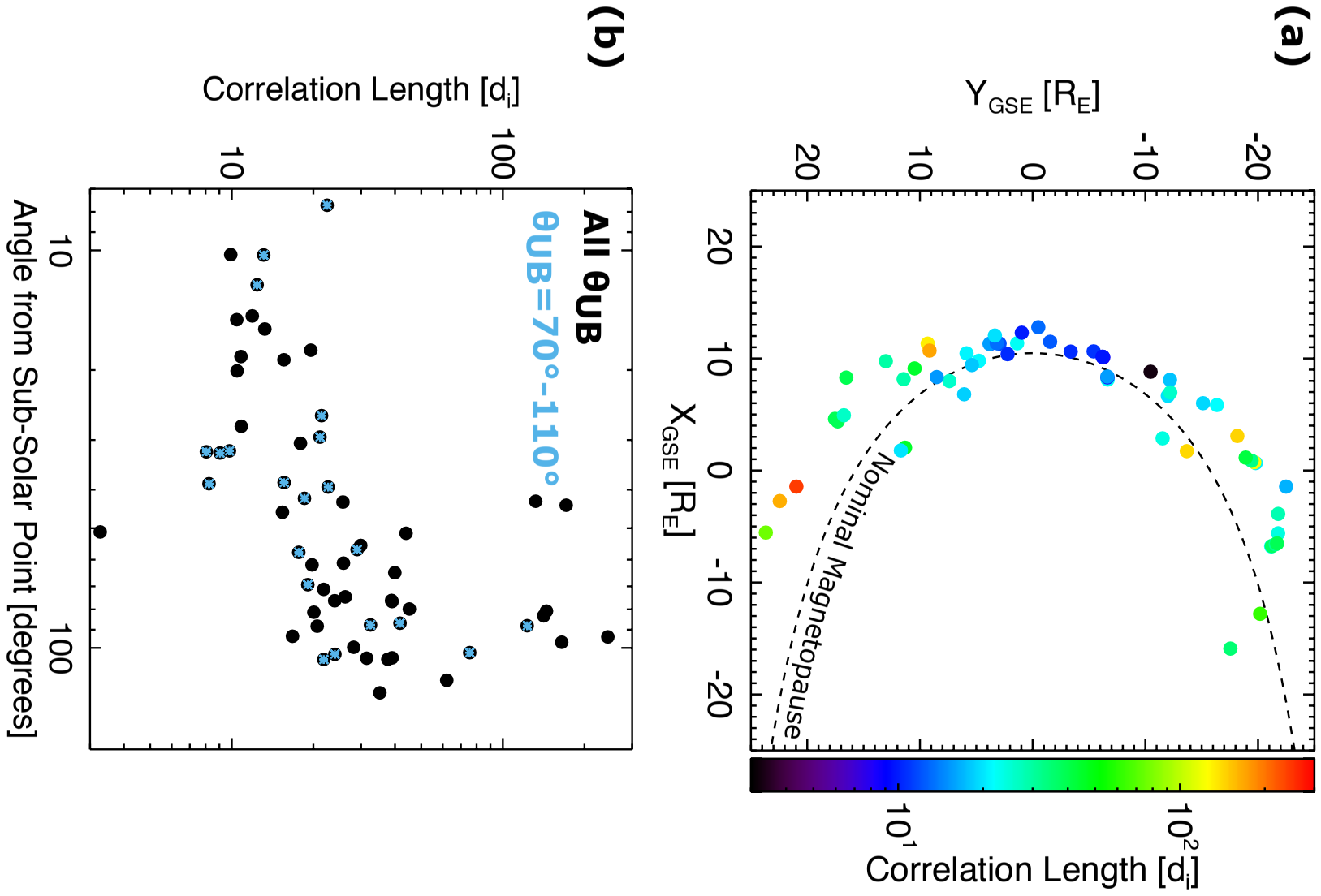

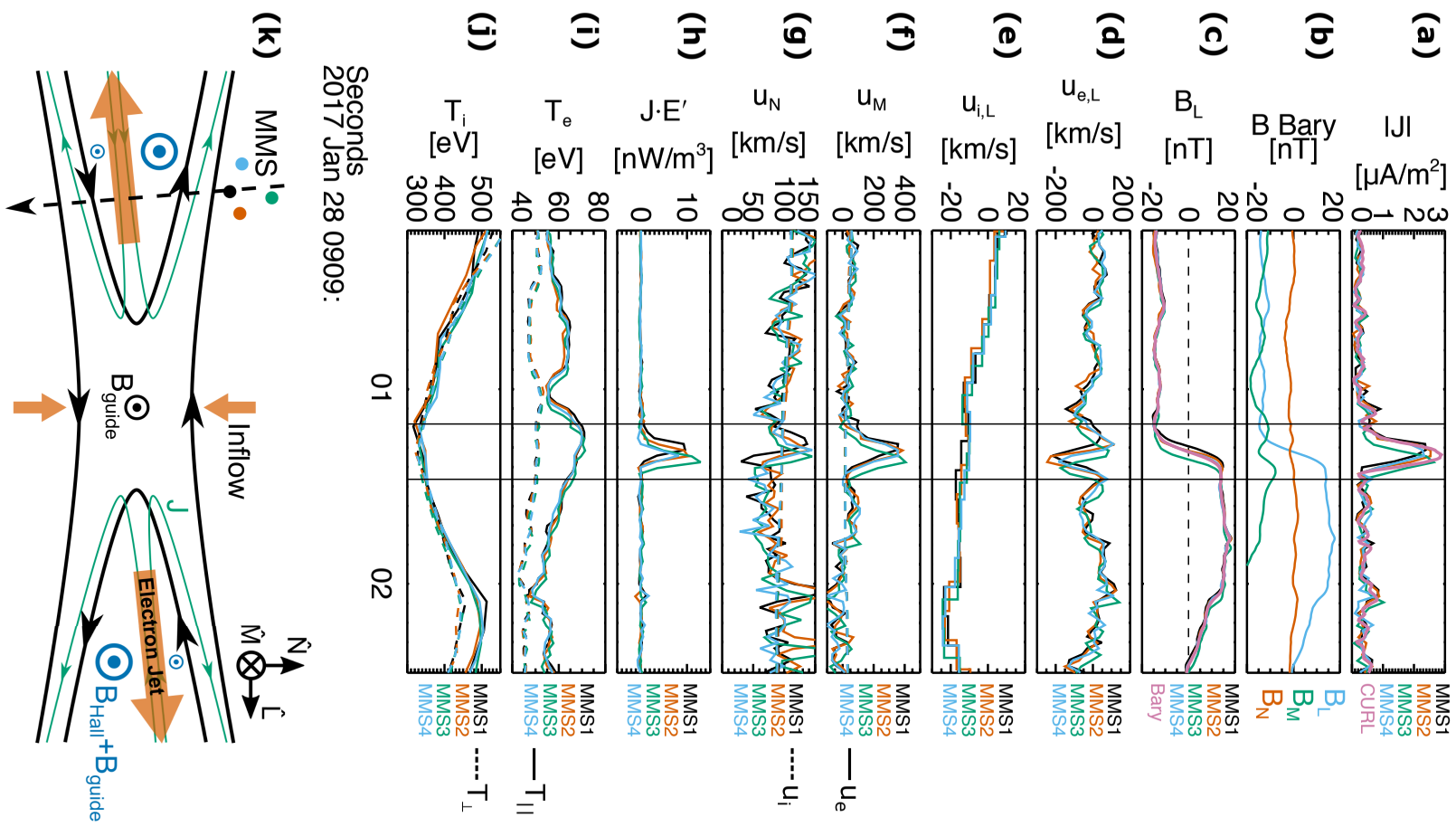

Physics of Plasmas

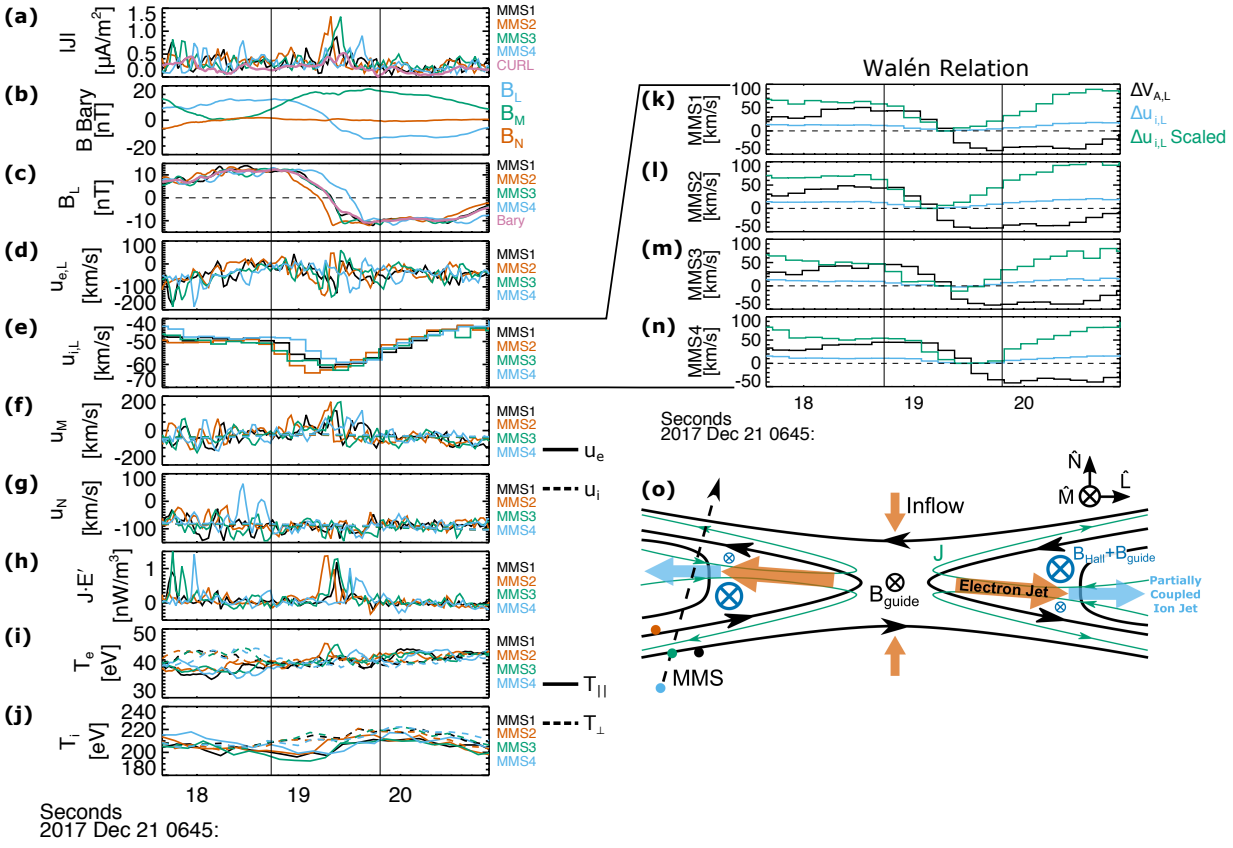

PLEASE CITE THIS ARTICLE AS DOI: 10.1063/5.0071106

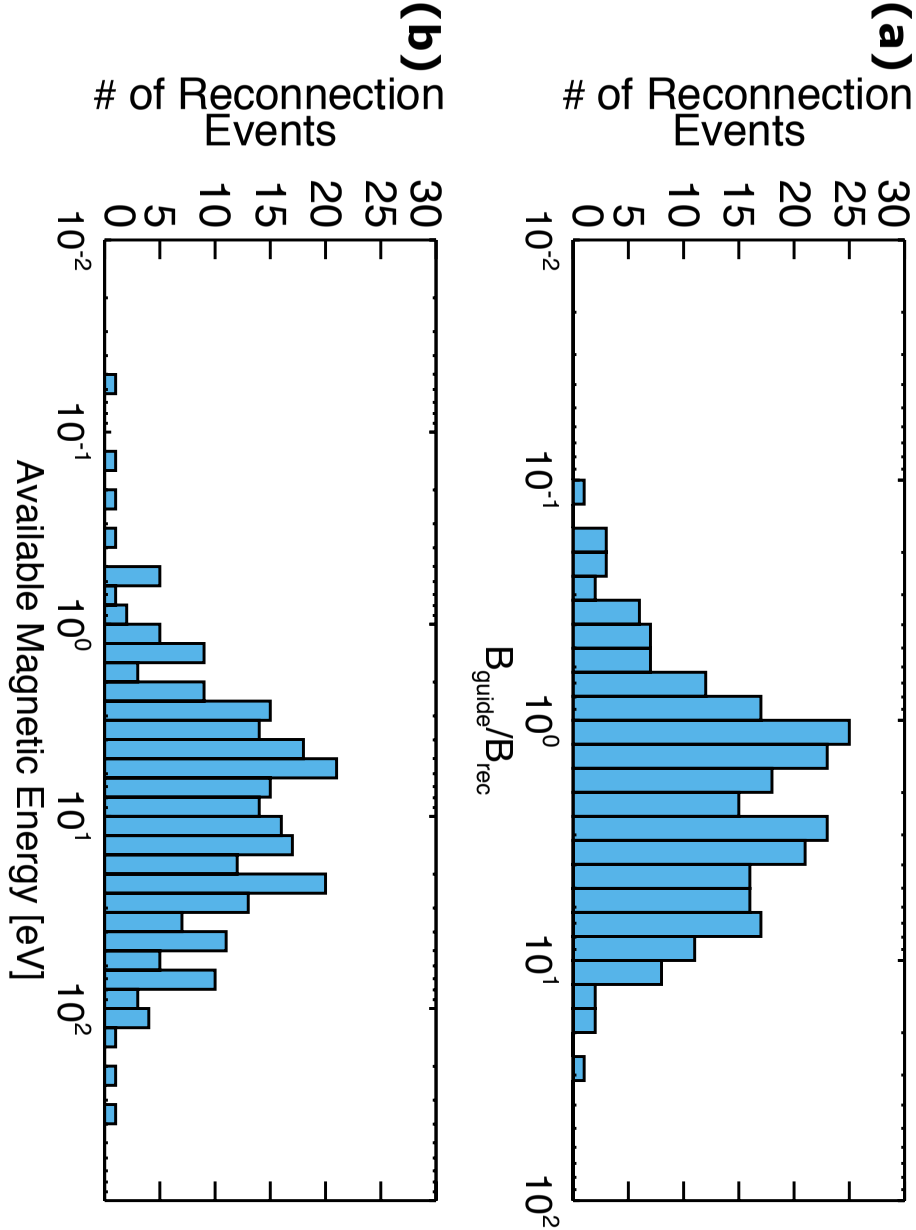

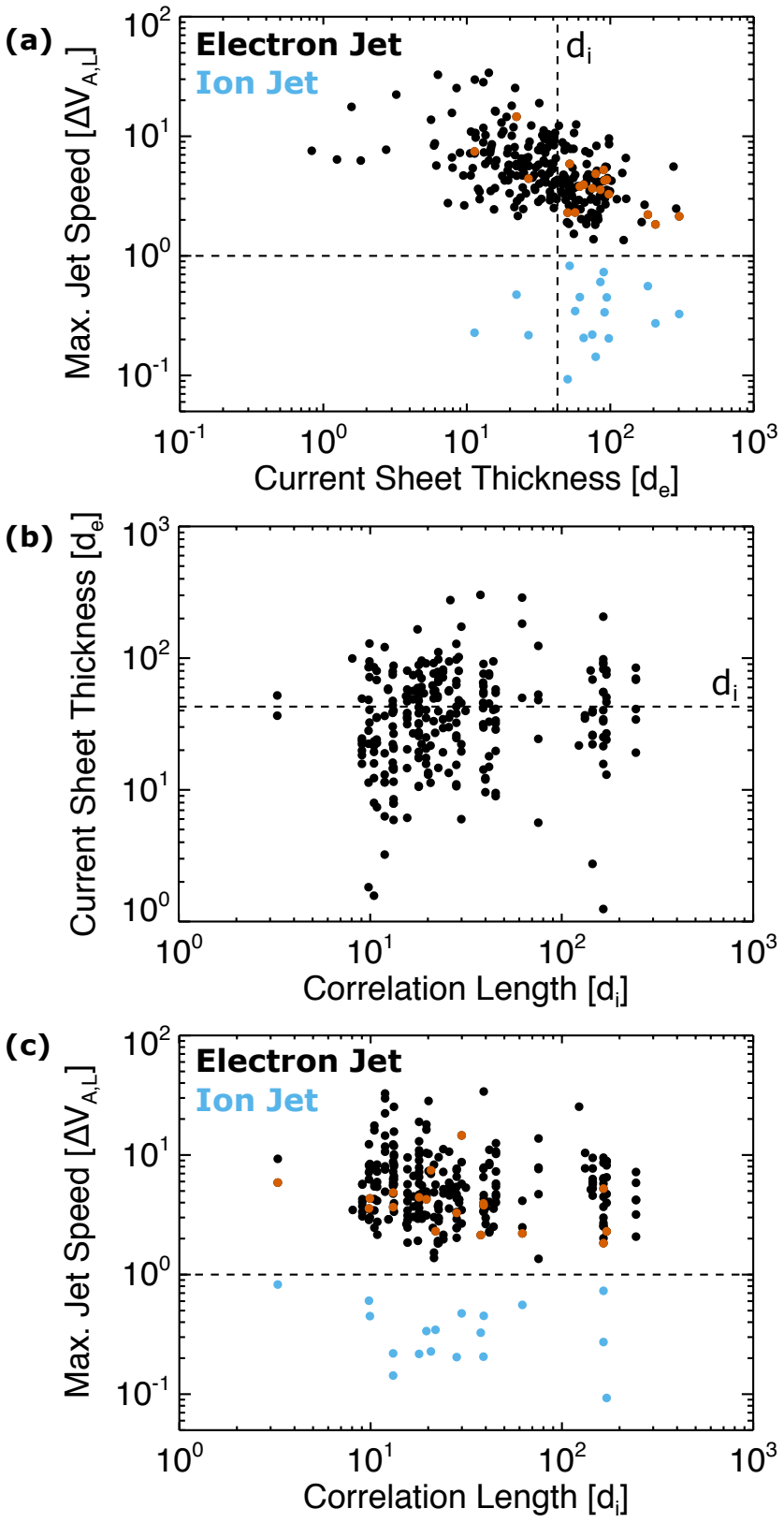

Physics of Plasmas